Сверхновые Звёзды:
Механизмы Взрыва и Моделирование

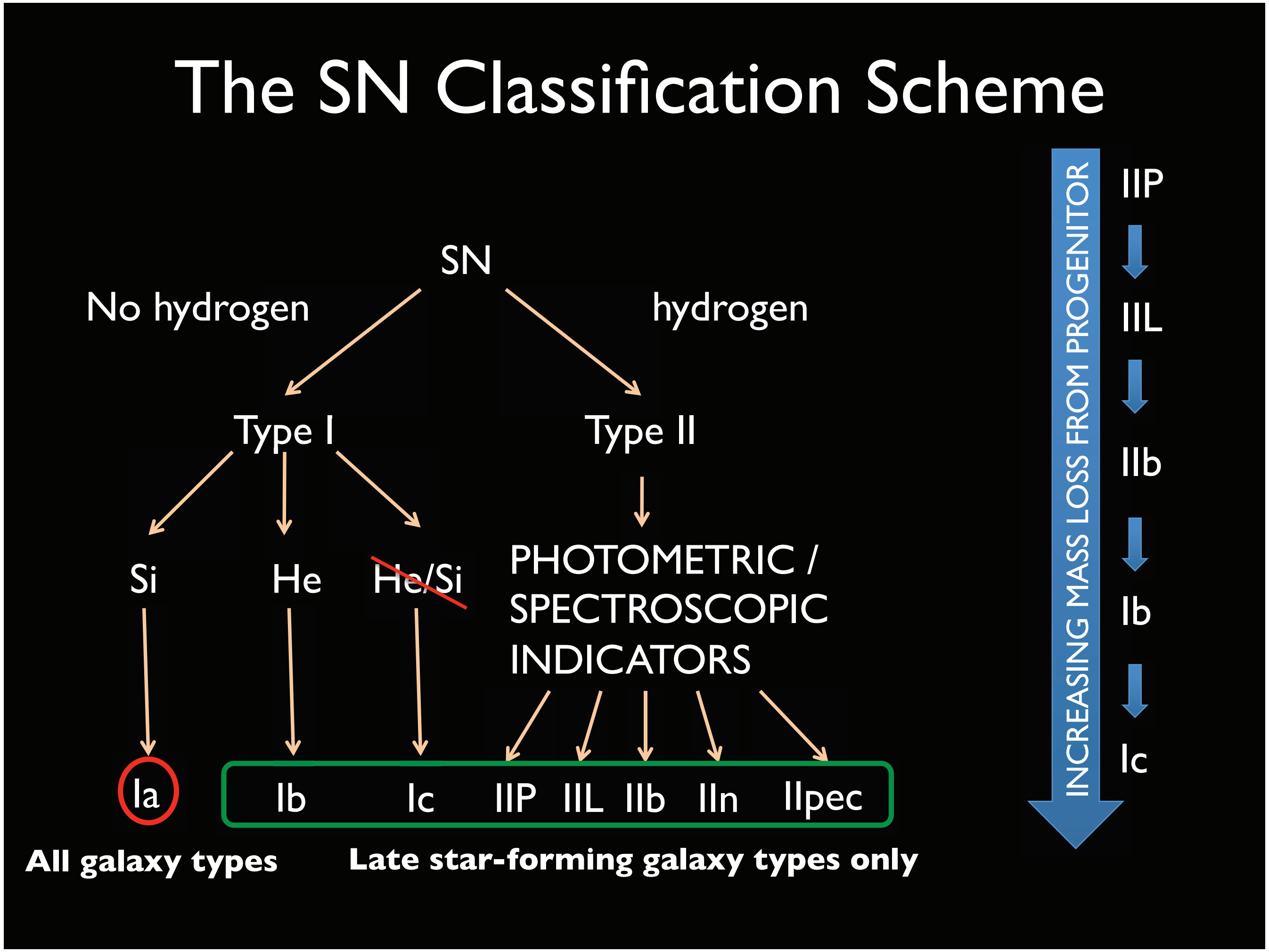

Maund (2012)

H-R diagram with 2 $M_\odot$ evolution track

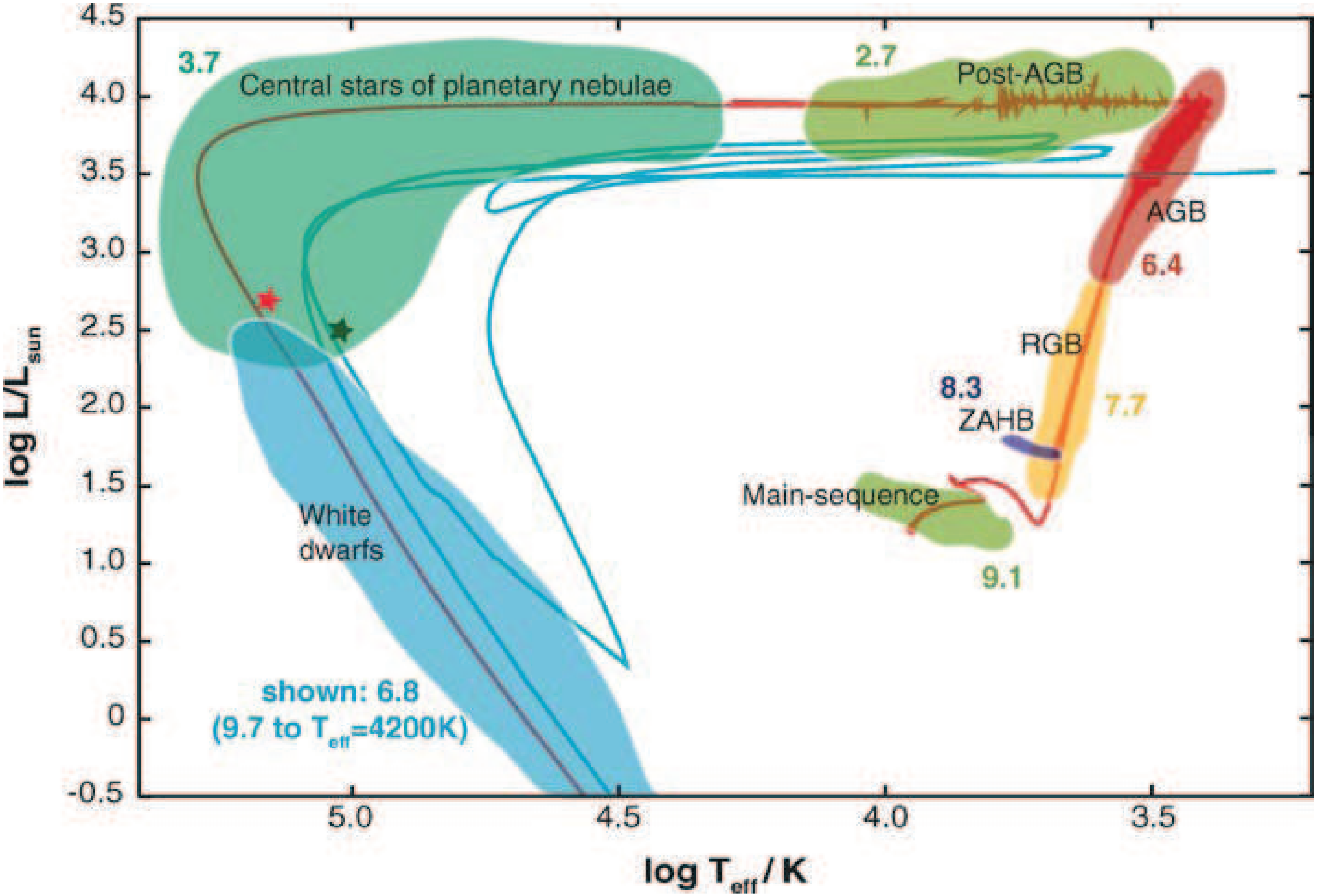

Herwig (2005)

H-R diagram for 8-100 $M_\odot$ stars

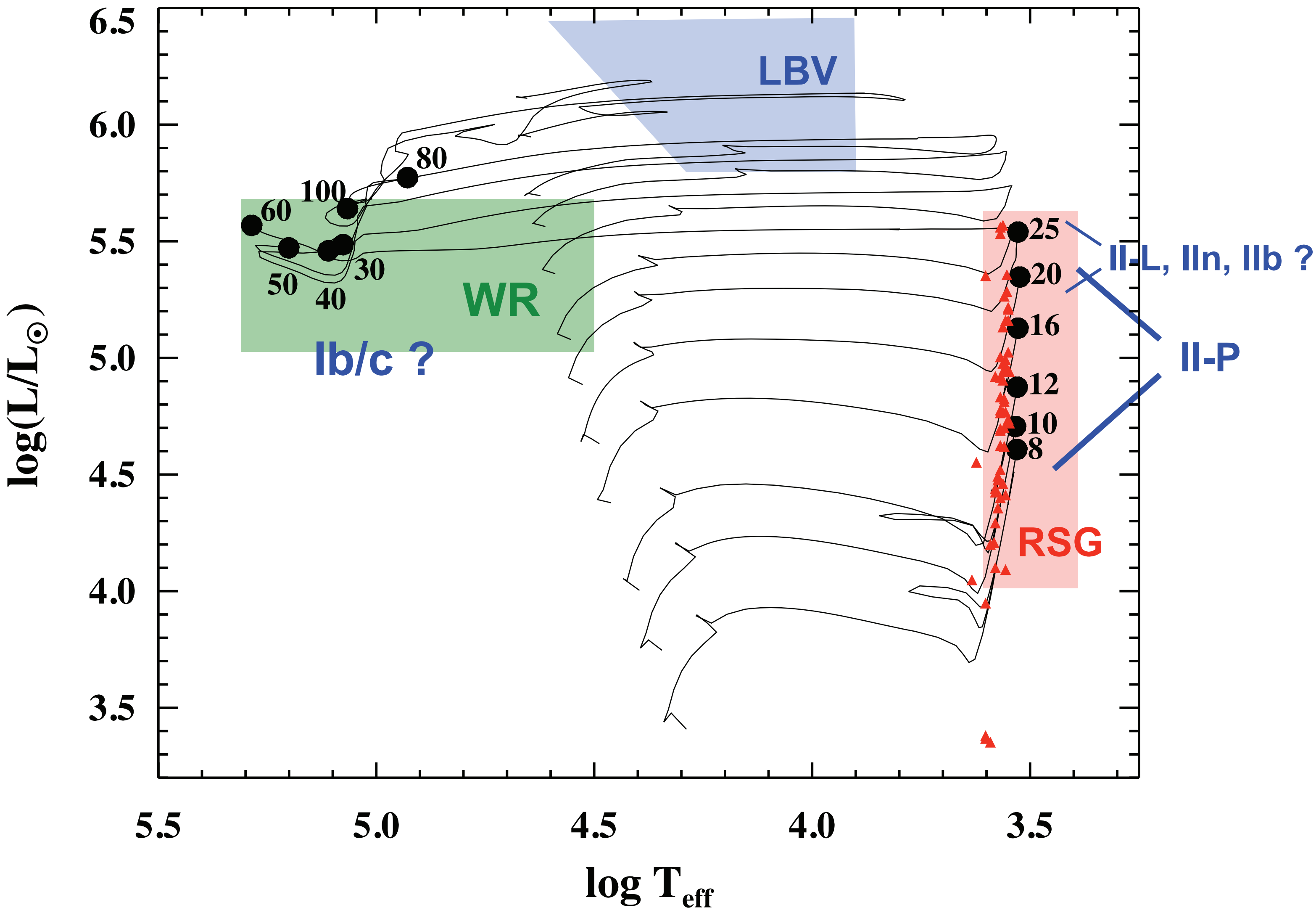

Leonard (2011)

Evolutionary tracks in the $T_c - \rho_c$ plane

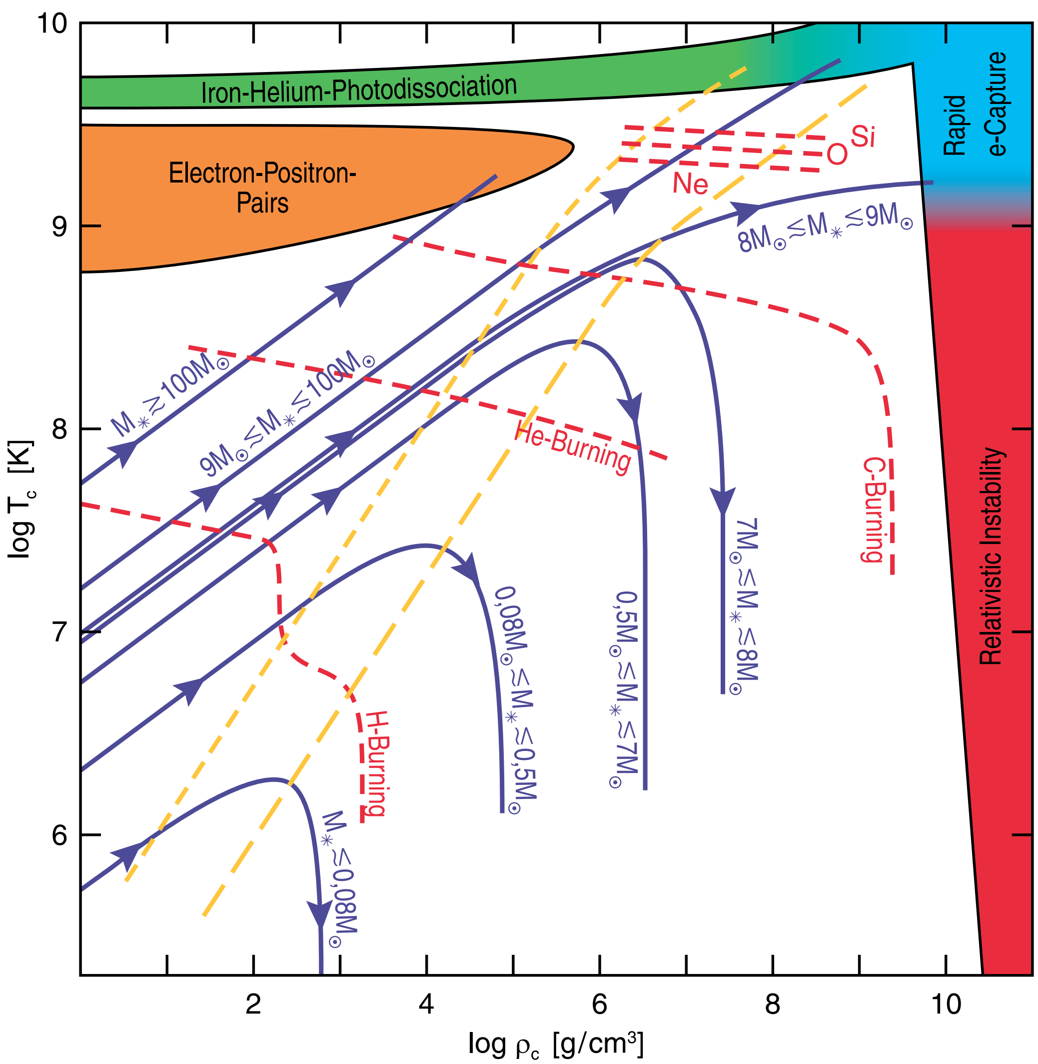

Janka (2012)

Mass distributions for white dwarfs

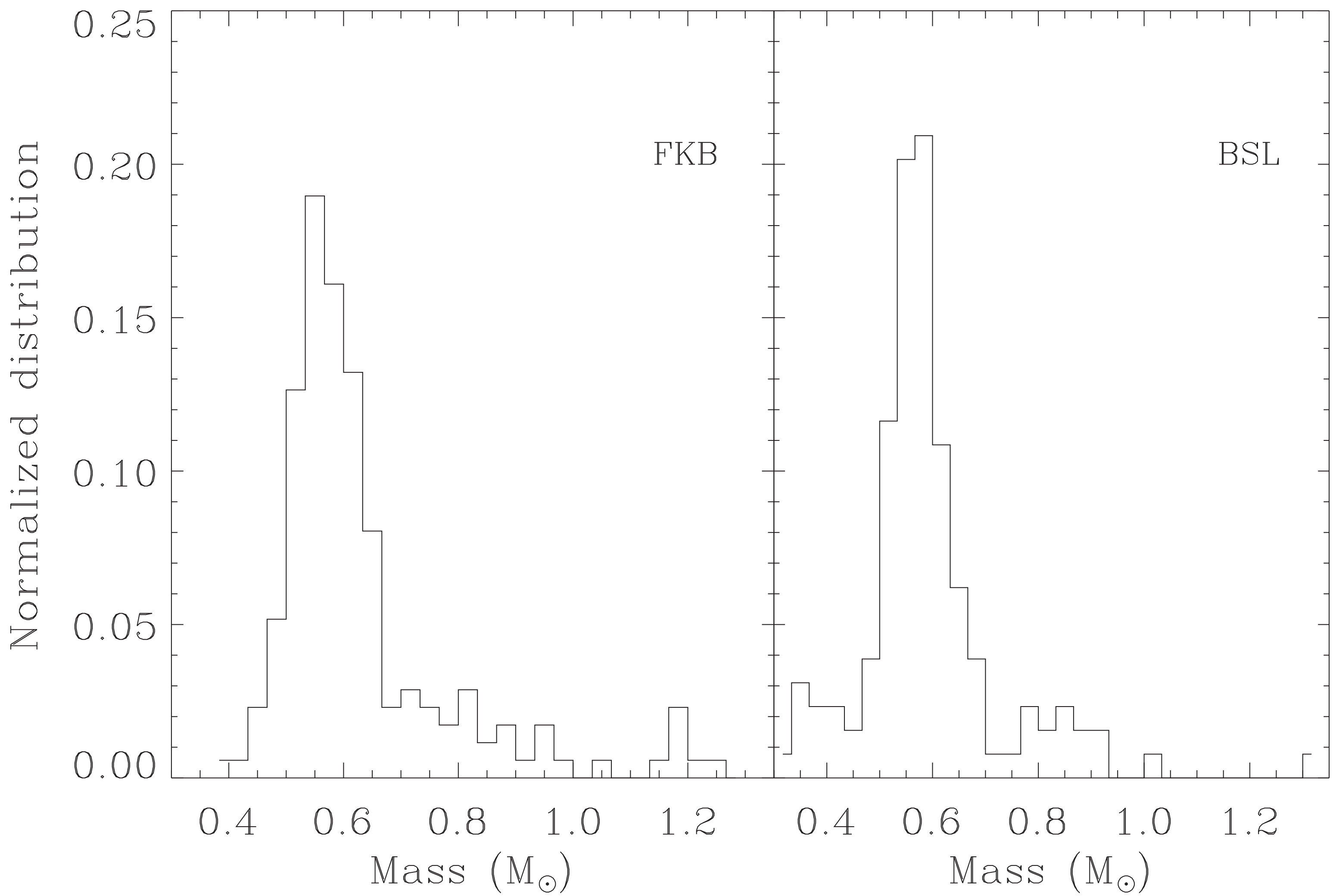

Finley et al. (1997)

The Chandrasekhar limit for non-rotating WDs

Chandrasekhar (1931):

THE MAXIMUM MASS OF IDEAL WHITE DWARFS

By S. CHANDRASEKHAR

ABSTRACT

The theory of the *polytropic gas spheres* in conjunction with the equation of state of a *relativistically degenerate electron-gas* leads to a *unique value for the mass of a star* built on this model. This mass ($=0.91\odot$) is interpreted as representing the upper limit to the mass of an ideal white dwarf.

The modern value is $M_{\mathrm{Ch}} = 1.42\ (\frac{Y_e}{0.50})^2\ M_\odot$

Progenitor binaries for type Ia supernovae

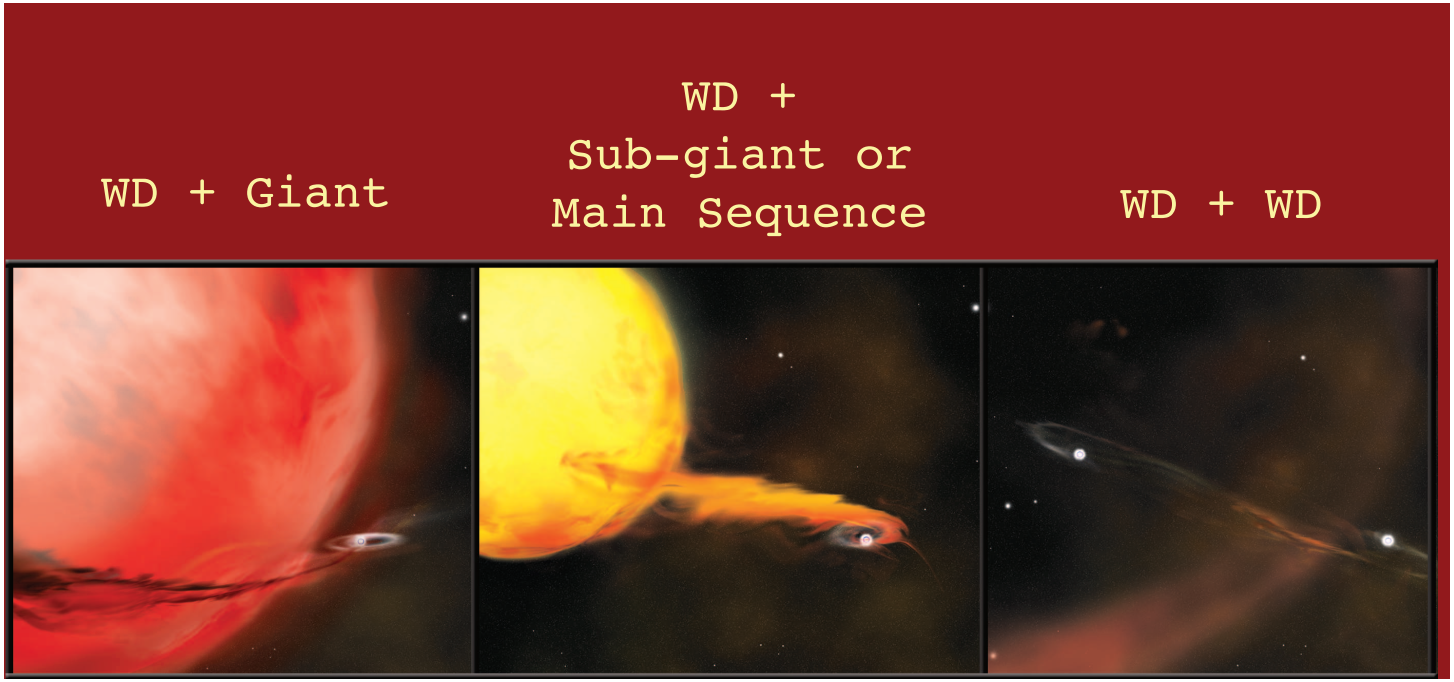

Chomiuk (2012)

Detonations

- M_{Ch} WD in hydrostatic equilibrium

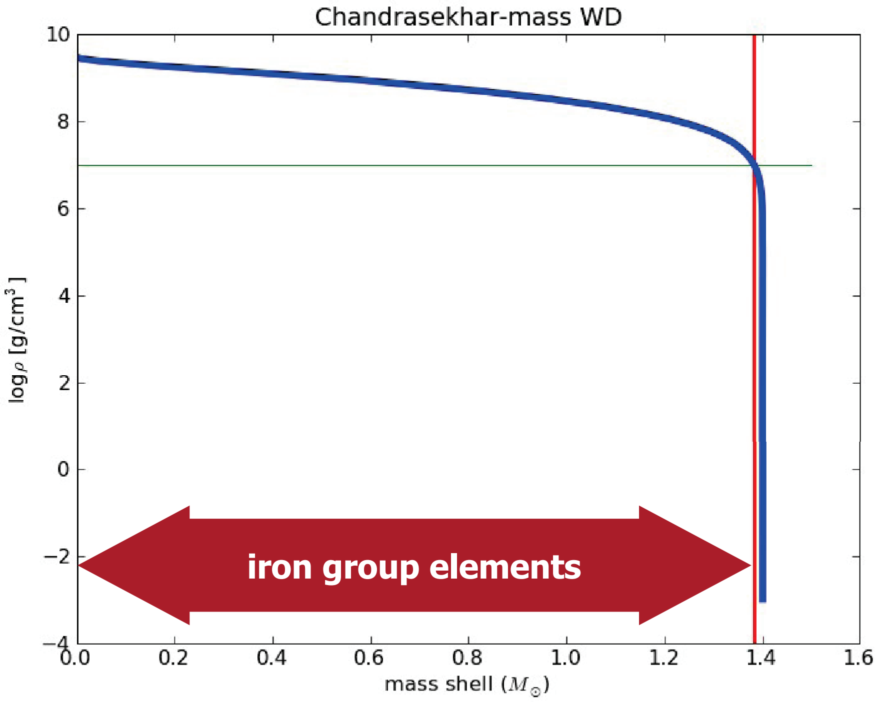

Roepke (2010)

Deflagrations

- subsonic bring WD material ahead of flame out of equilibrium
  pre-expansion

- laminar flames: Mach $\sim 10^{-2}$
  cannot catch up with WD expansion
  nuclear energy release insufficient

- buoyancy instabilities lead to
  turbulent combustion

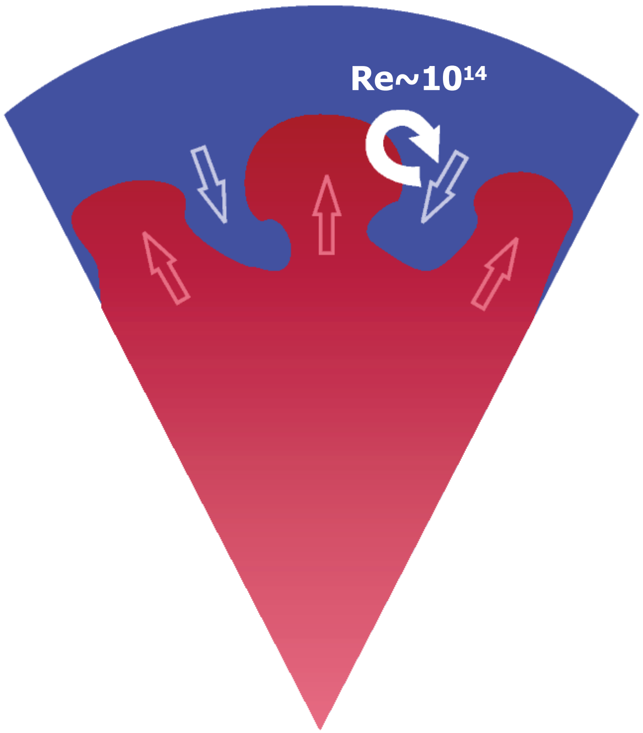

Roepke (2010)

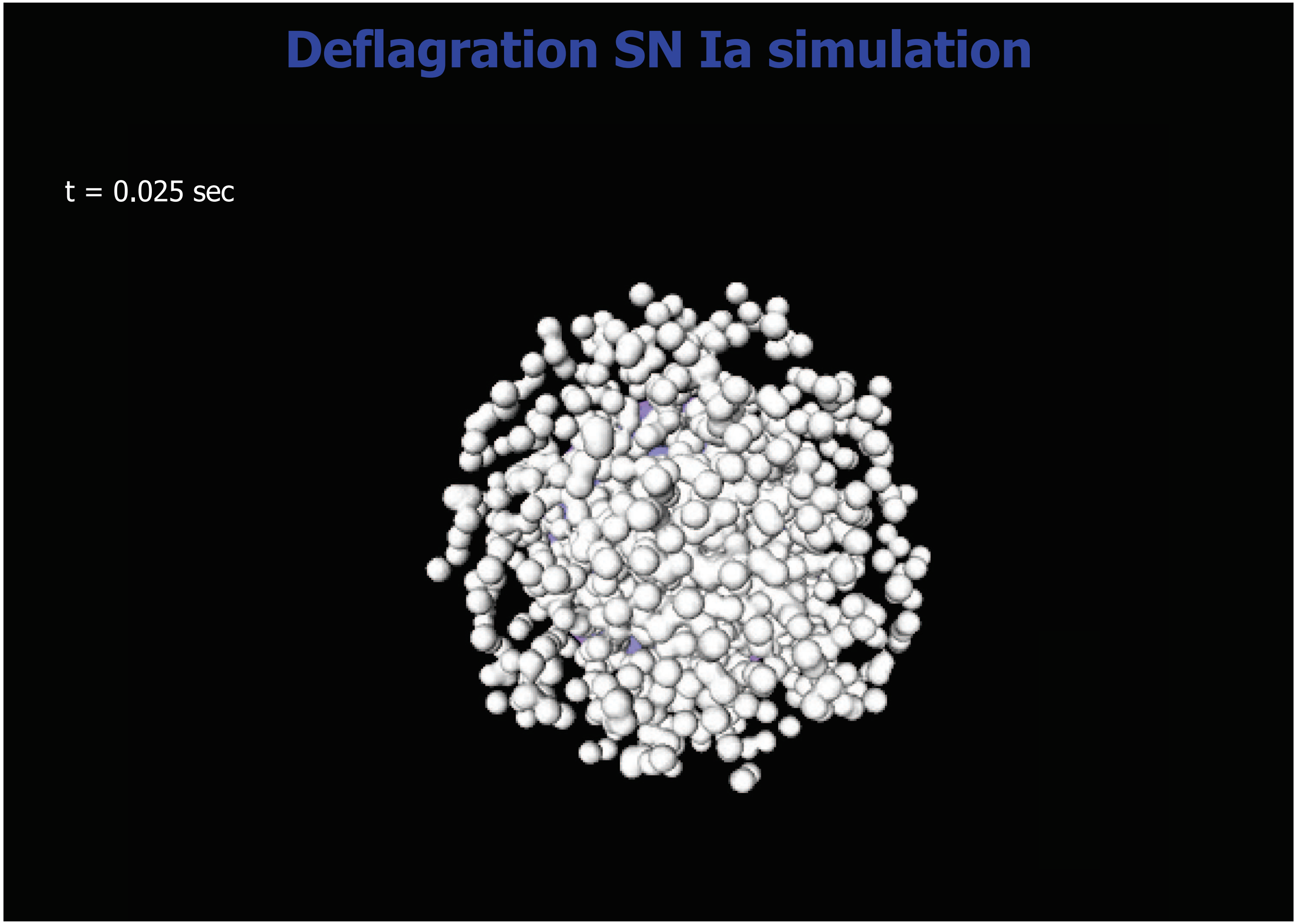

Roepke (2010)

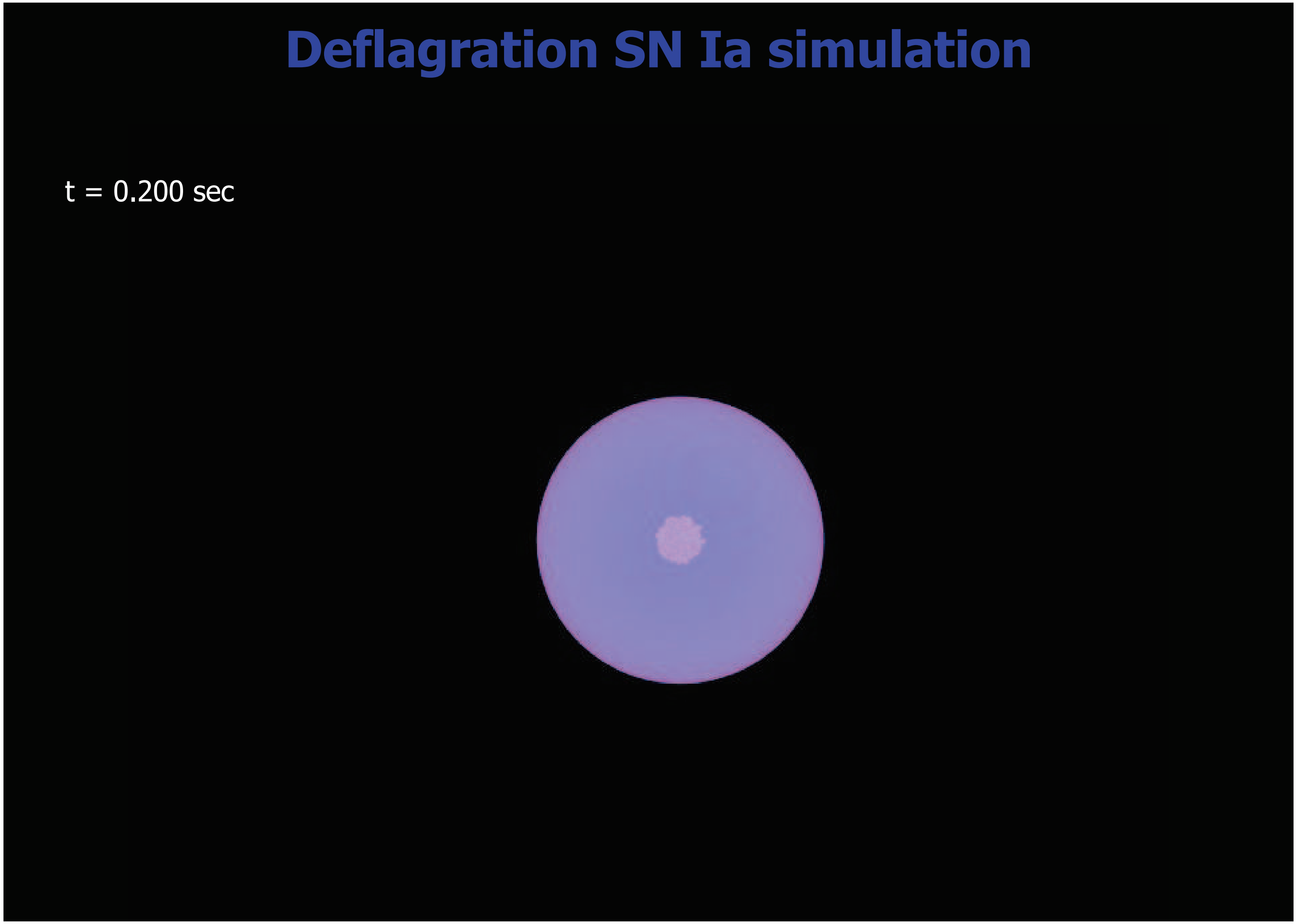

Roepke (2010)

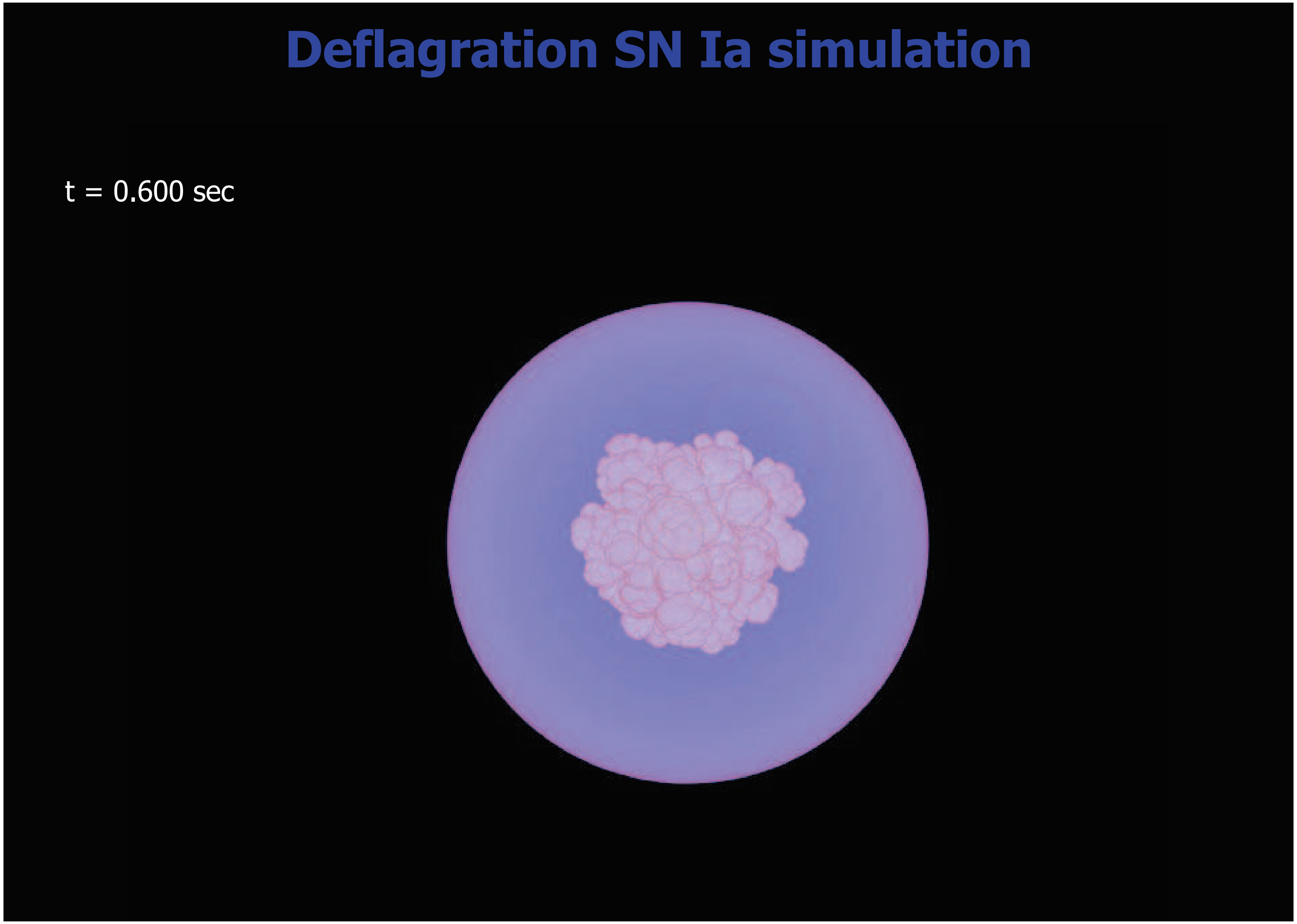

Roepke (2010)

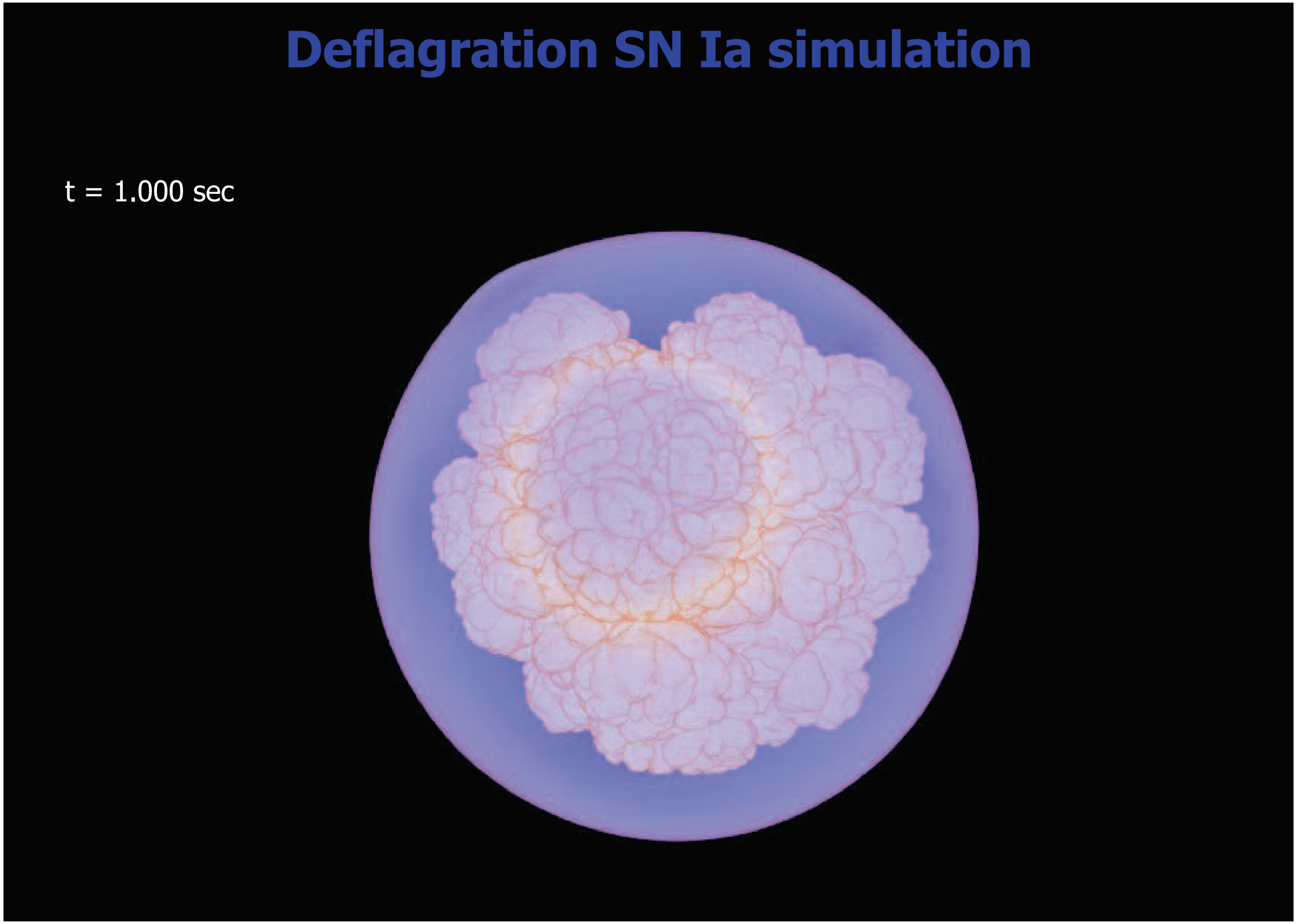

Roepke (2010)

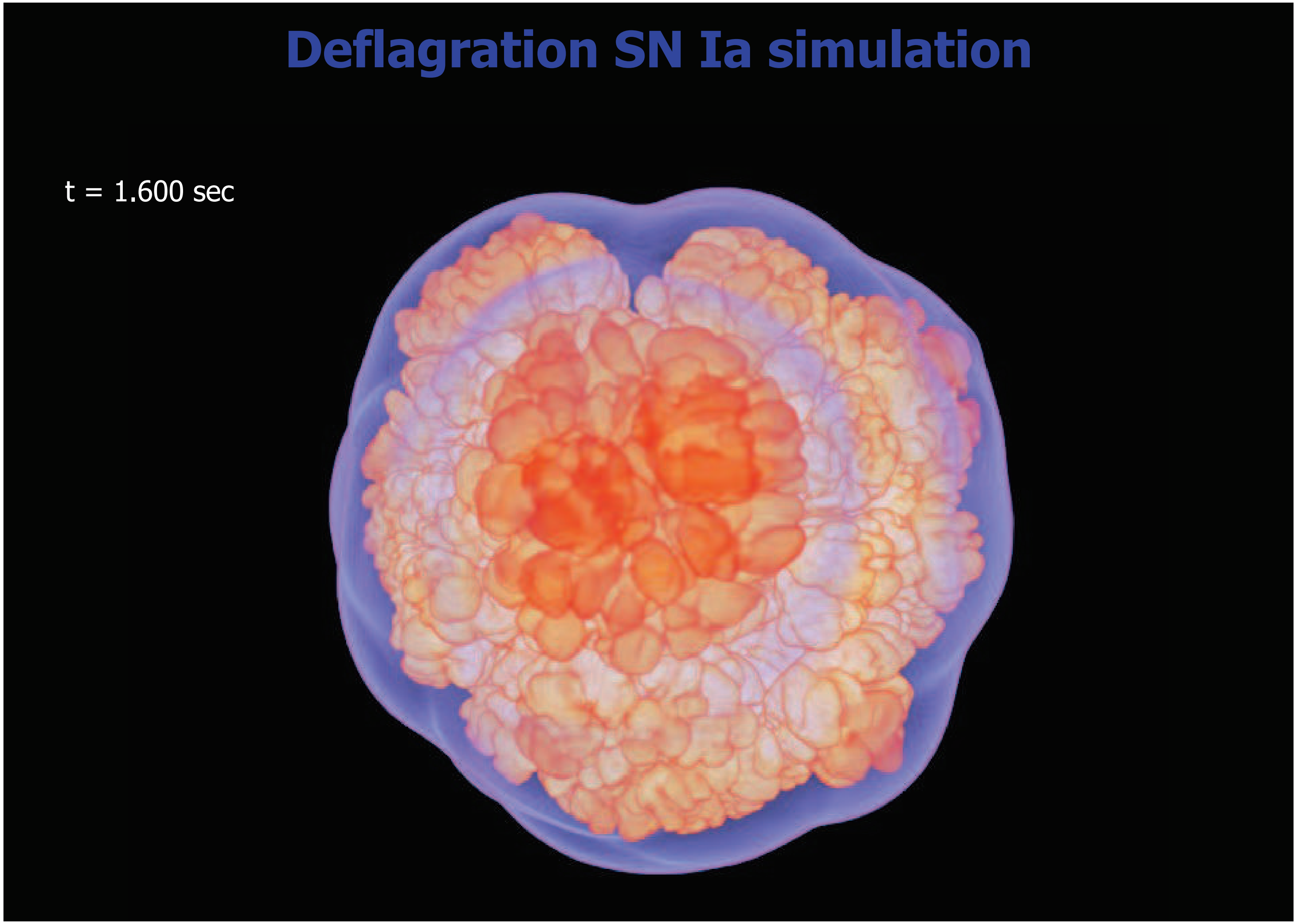

Roepke (2010)

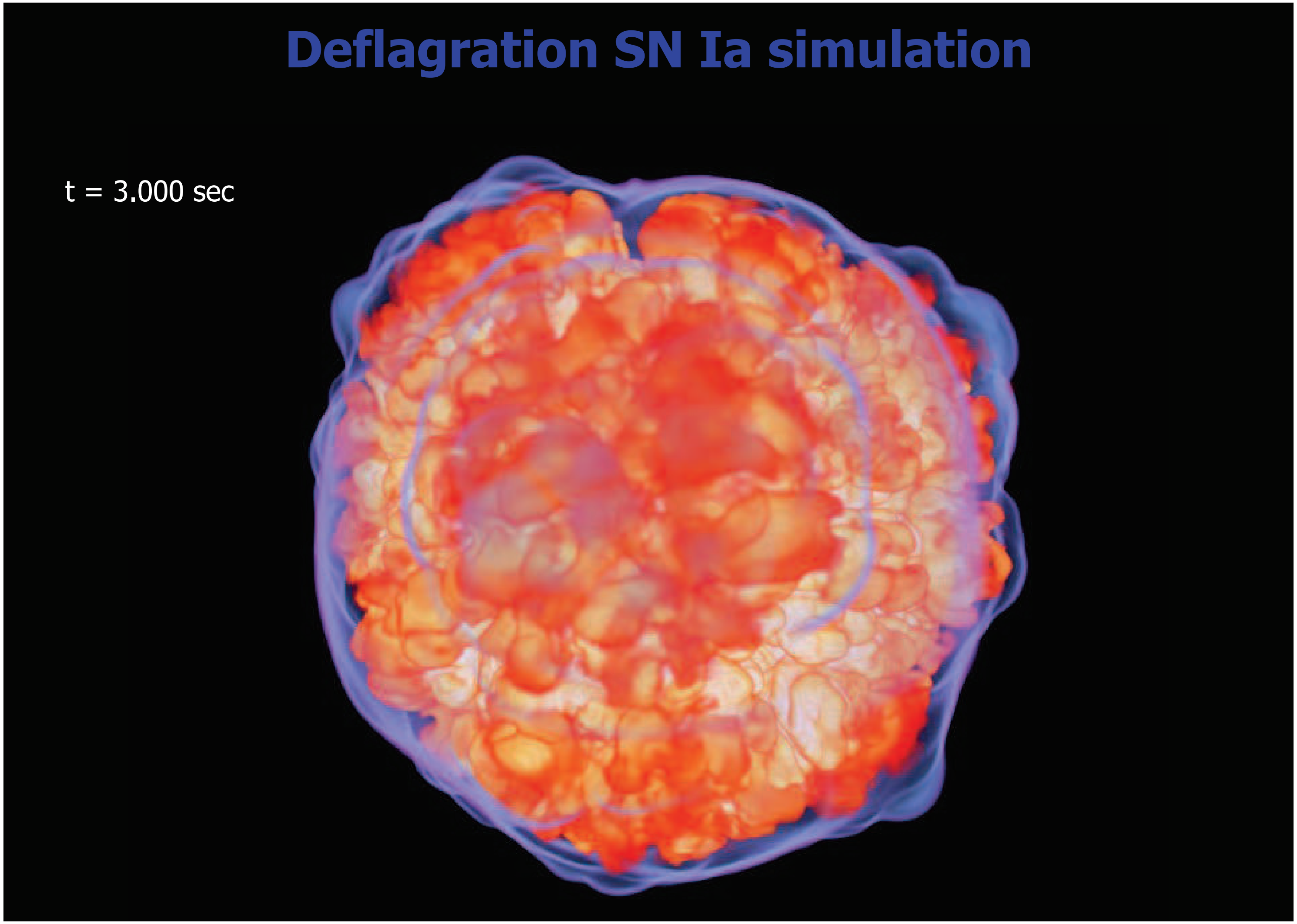

Roepke (2010)

Bolometric light curve

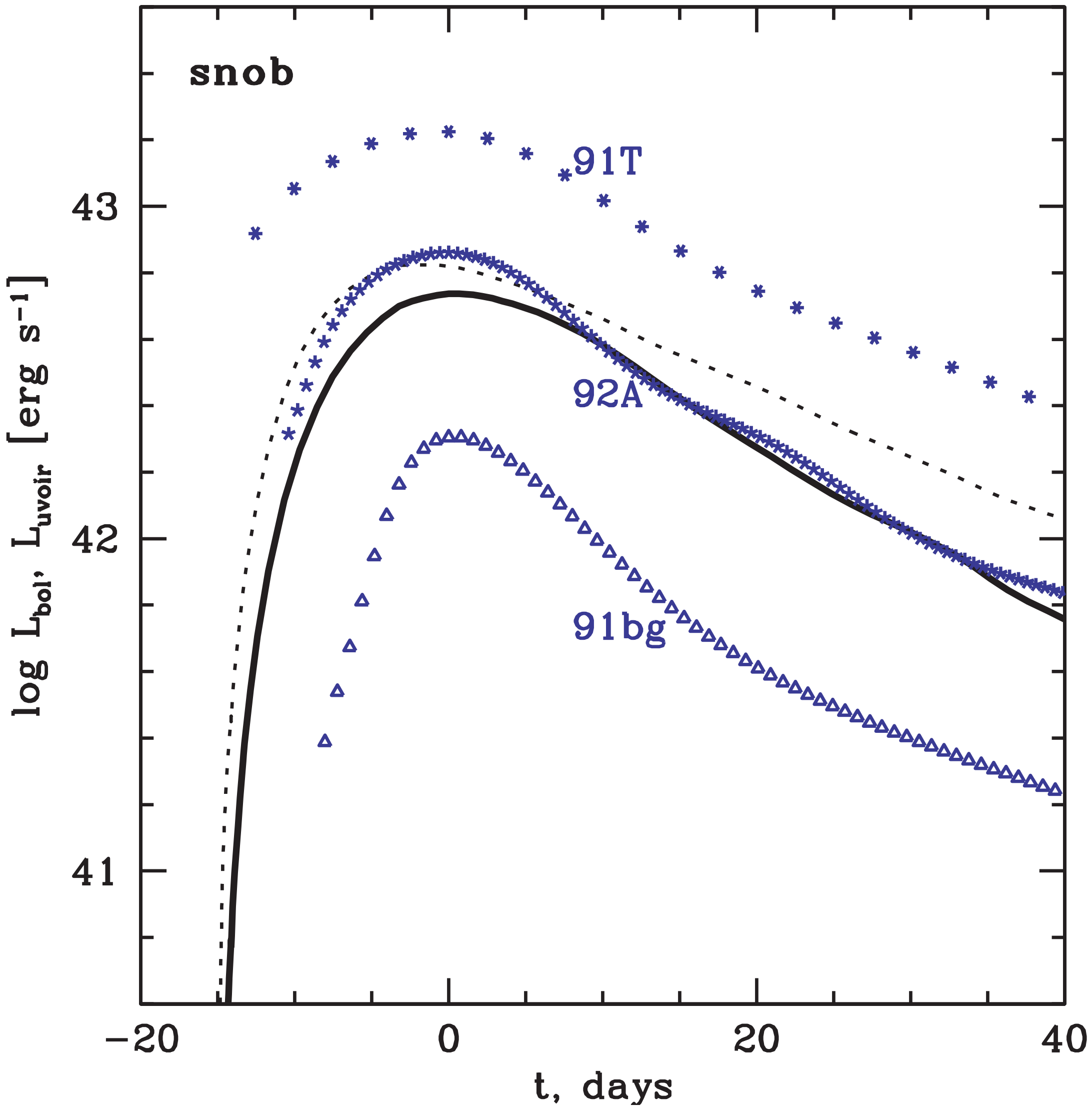

Roepke et al. (2007)

Detonation in sub-Ch. mass C+O white dwarf

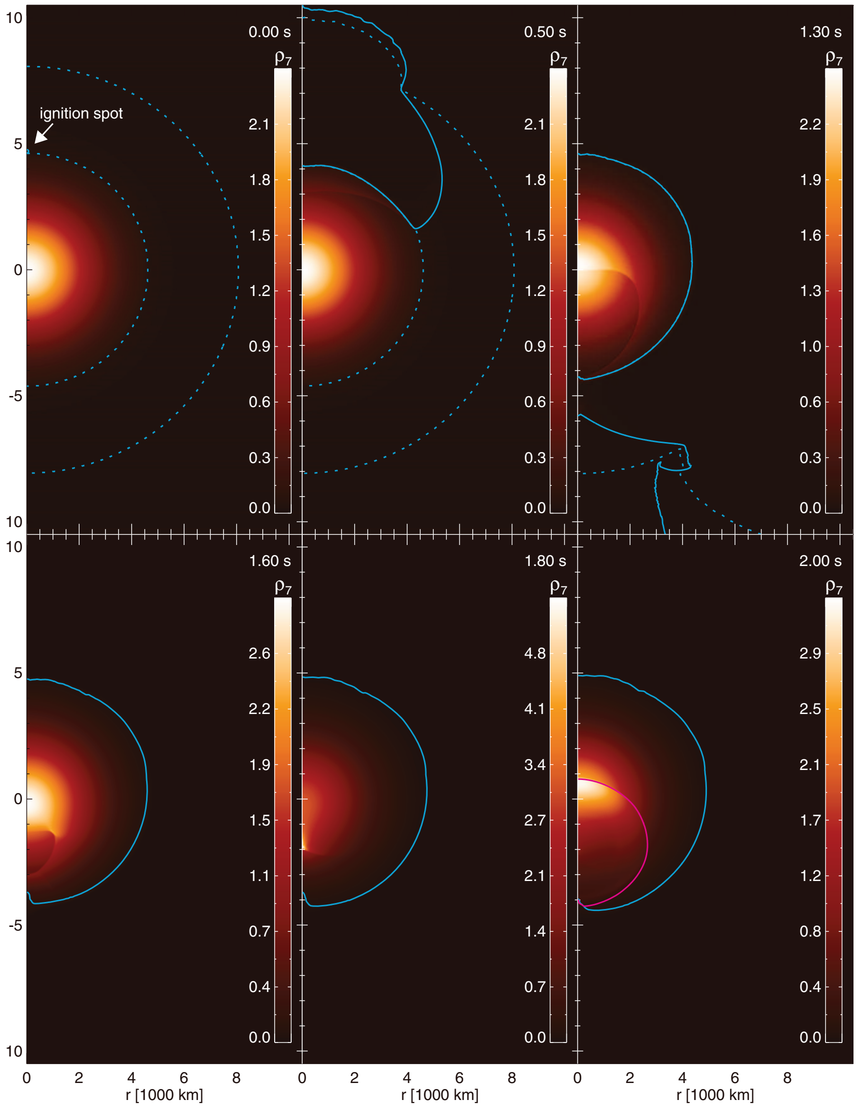

Fink et al. (2010)

Detonation in sub-Ch. mass C+O white dwarf

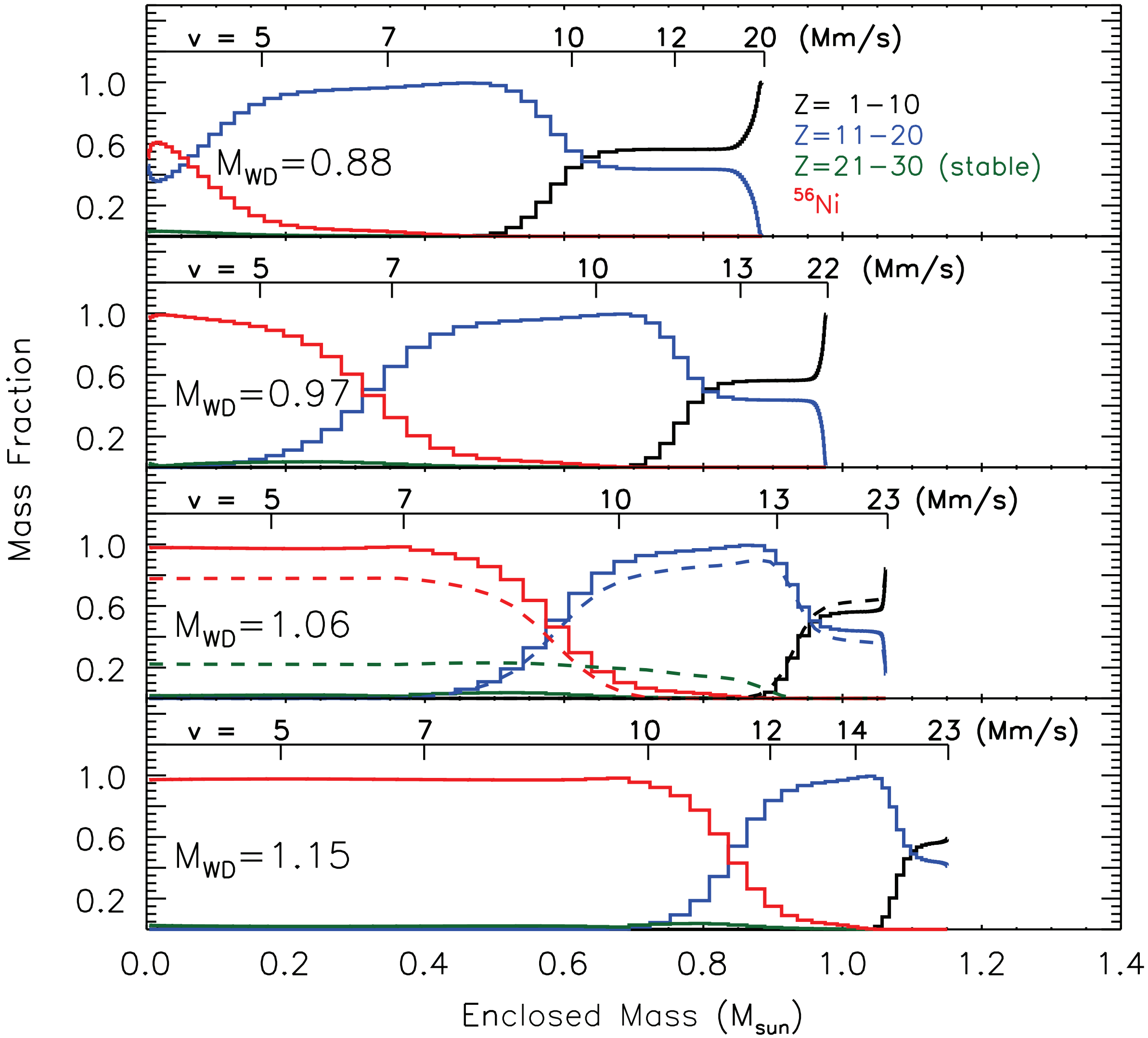

Sim et al. (2010)

Detonation in sub-Ch. mass C+O white dwarf

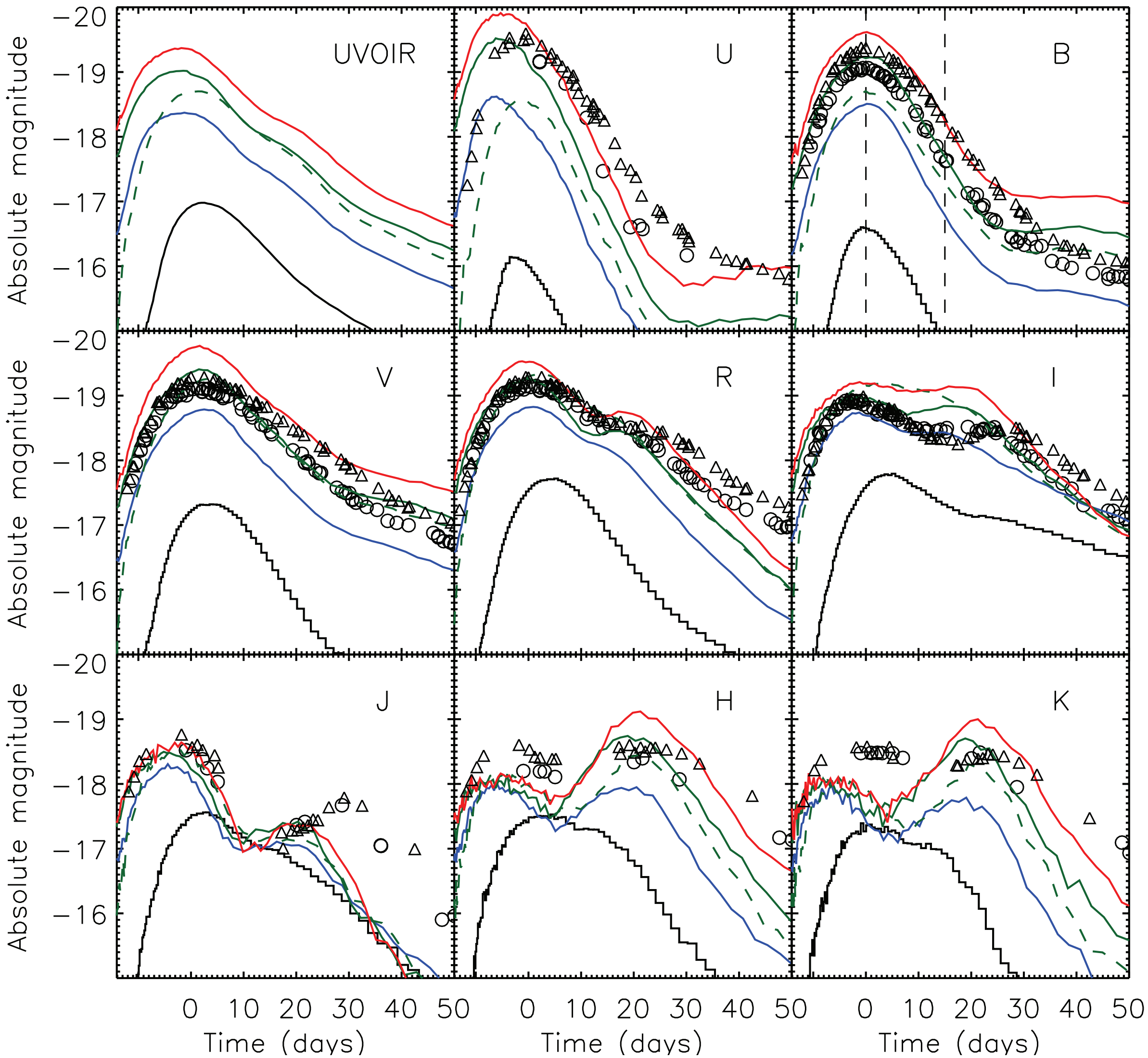

Sim et al. (2010)

Detonation in sub-Ch. mass C+O white dwarf

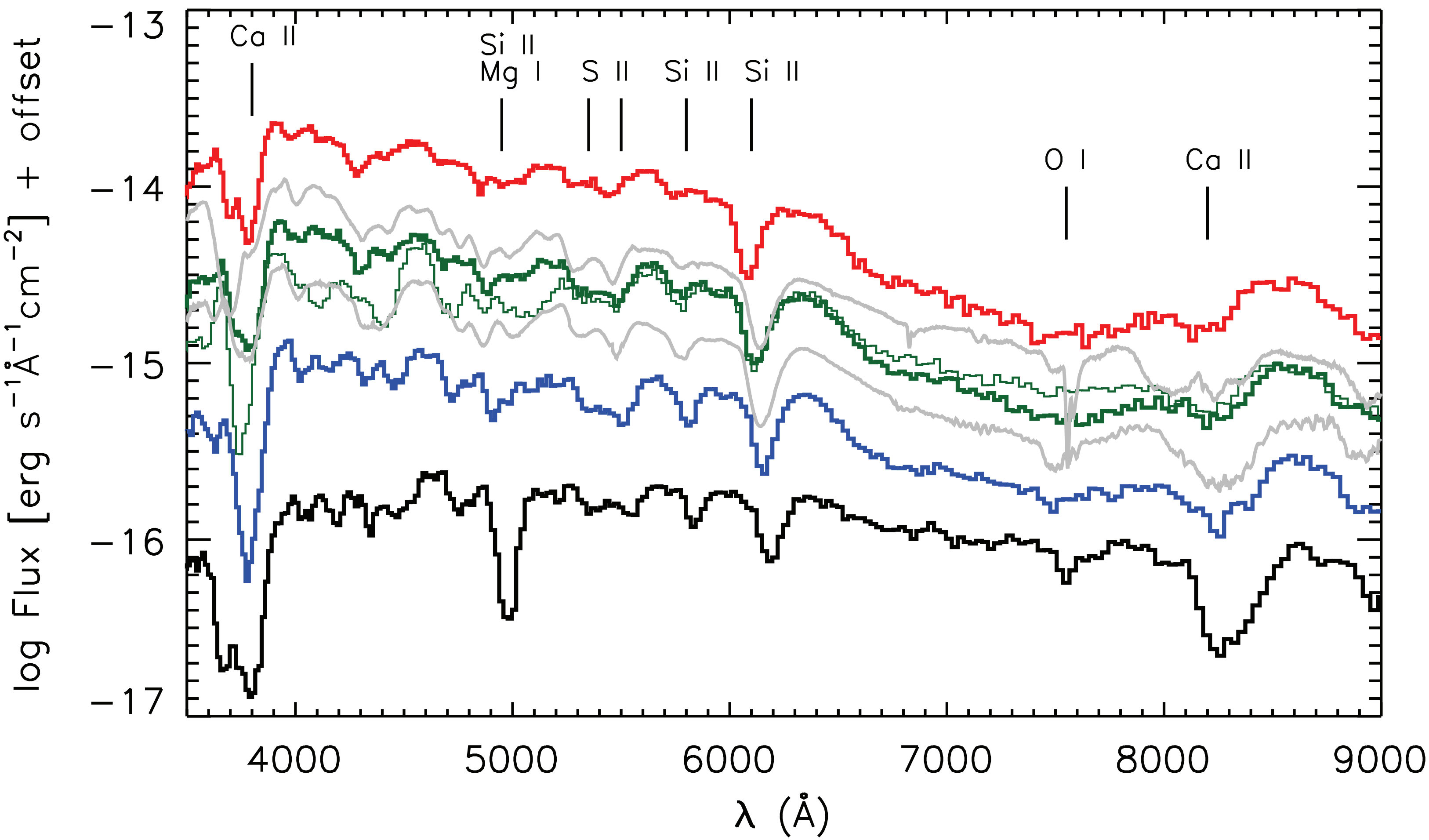

Sim et al. (2010)

Merger of 1.1 and 0.9 $M_\odot$ C–O white dwarfs

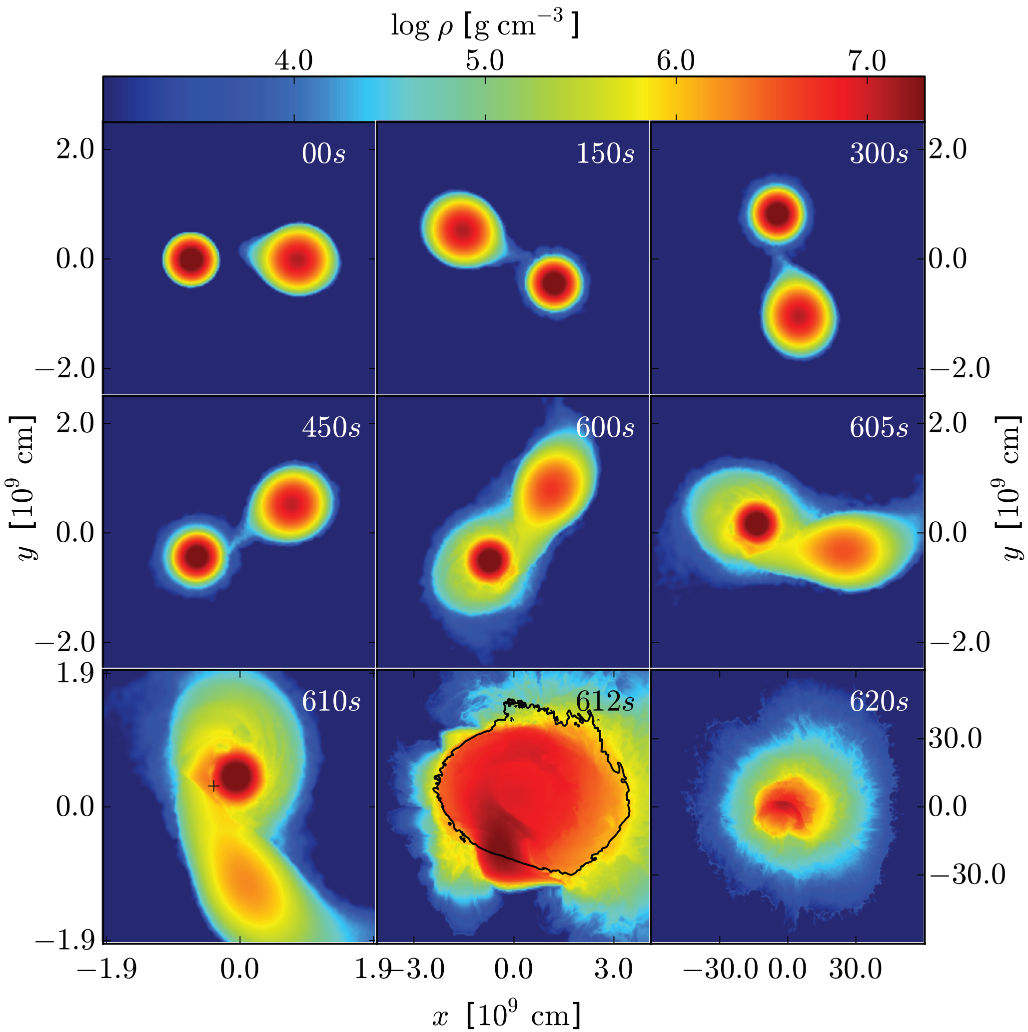

$E_{kin} = 1.7 \times 10^{51}$ erg, and $M_{\rm Ni} = 0.62\ M_\odot$.

Pakmor et al. (2012)

Merger of 1.1 and 0.9 $M_\odot$ C–O white dwarfs

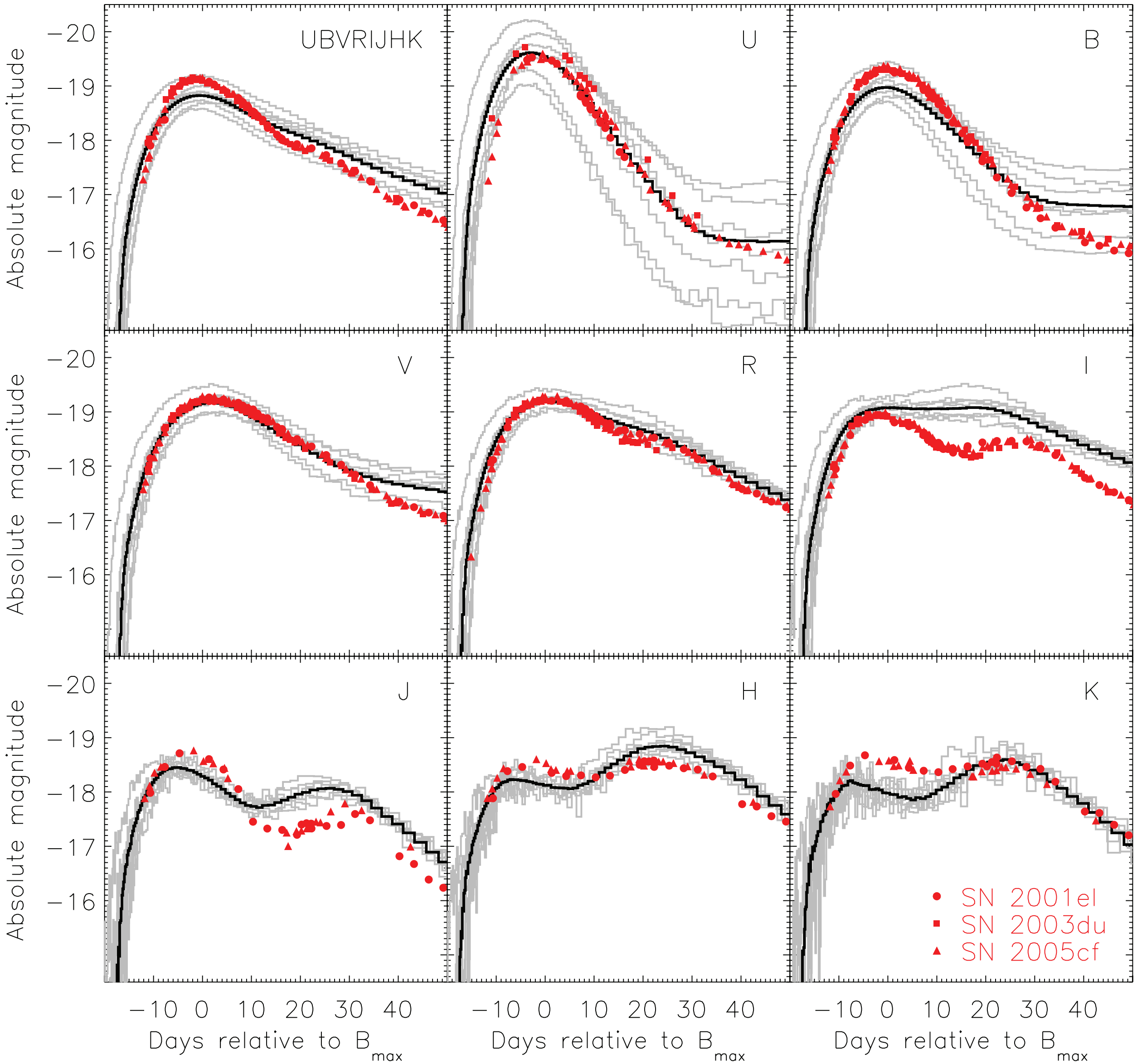

Pakmor et al. (2012)

Merger of 1.1 and 0.9 $M_\odot$ C–O white dwarfs

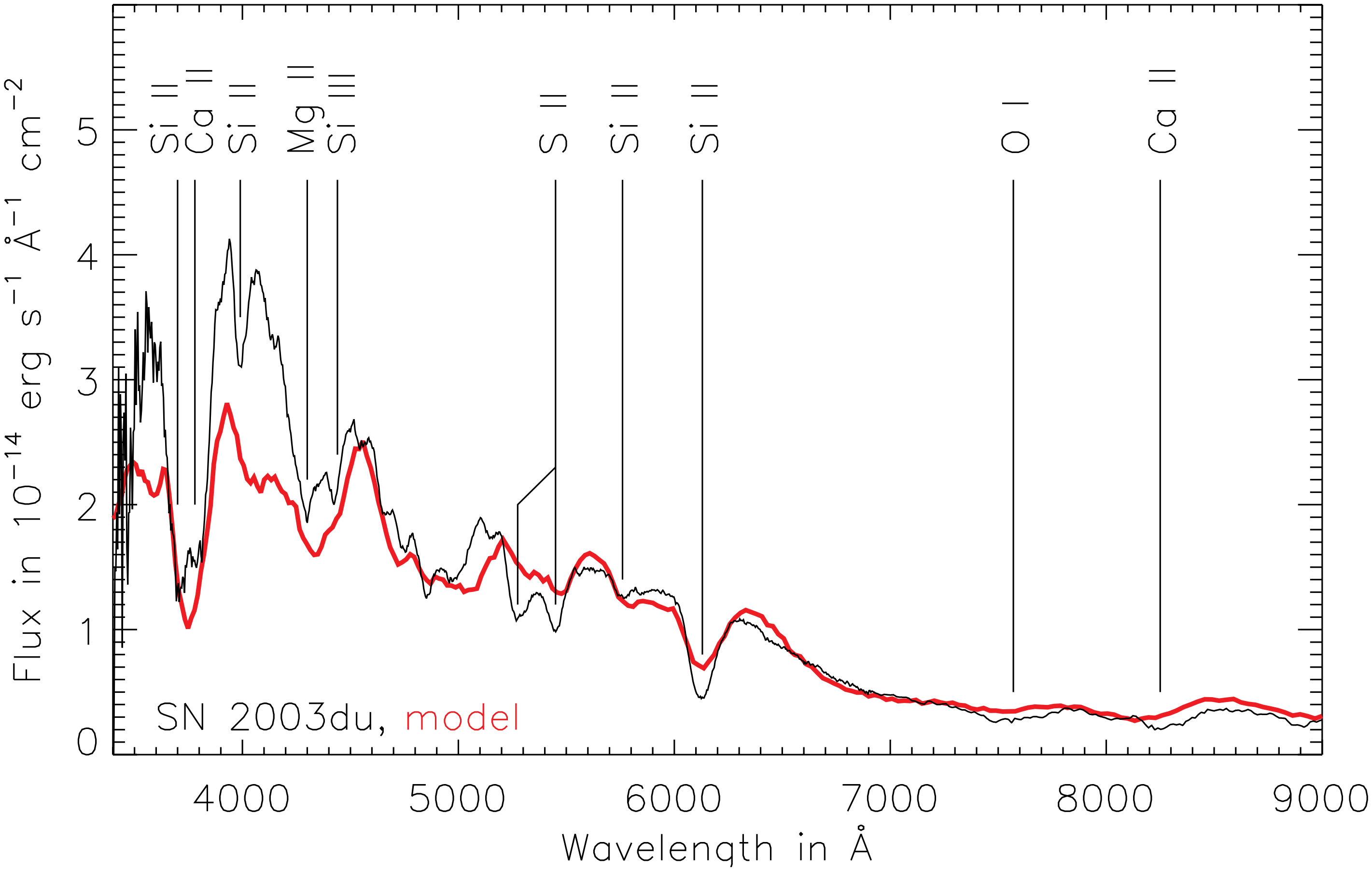

Pakmor et al. (2012)

Constraints on the SN 2014J progenitor system

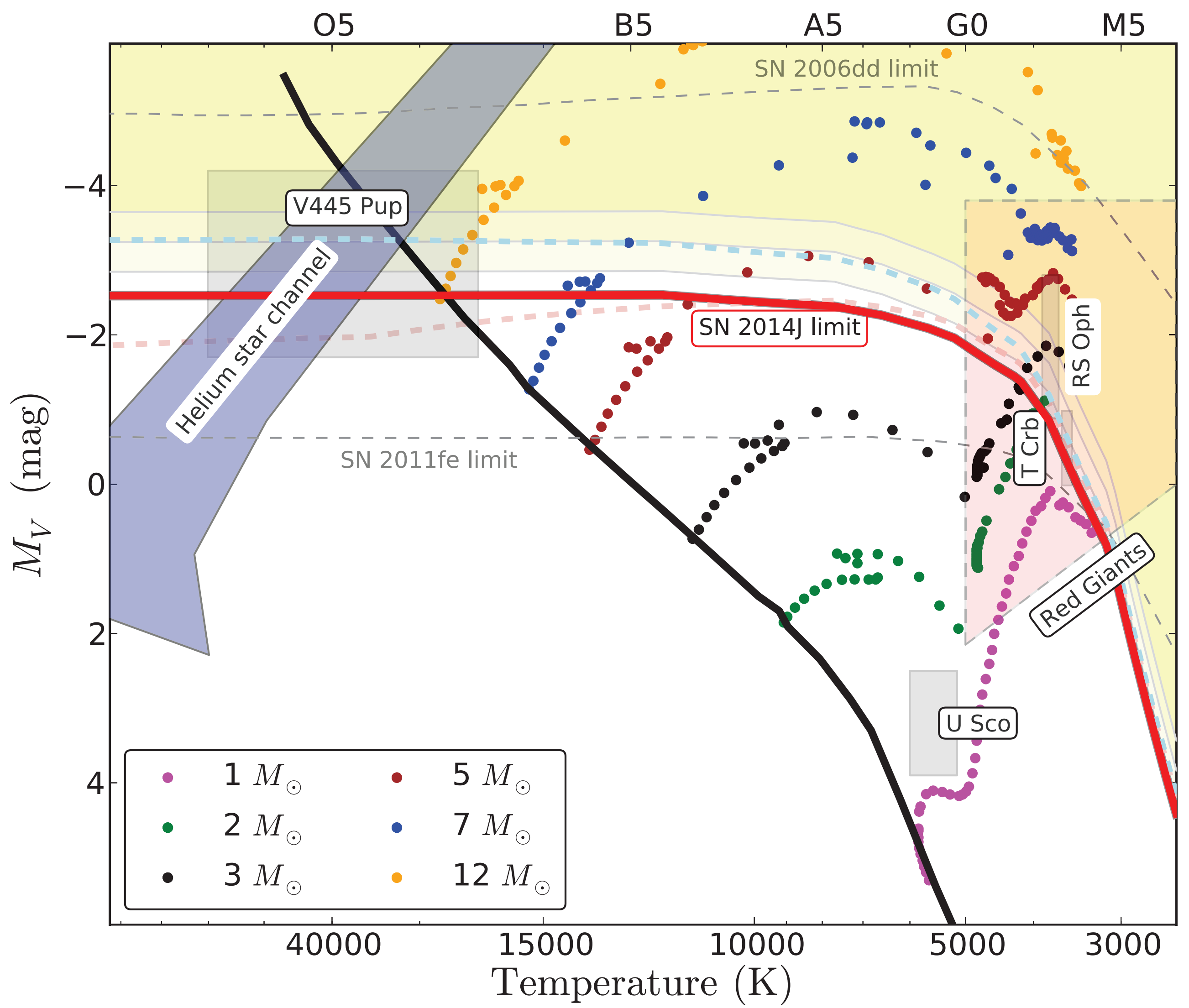

Kelly et al. (2014)

Direct Collisions of White-Dwarfs?

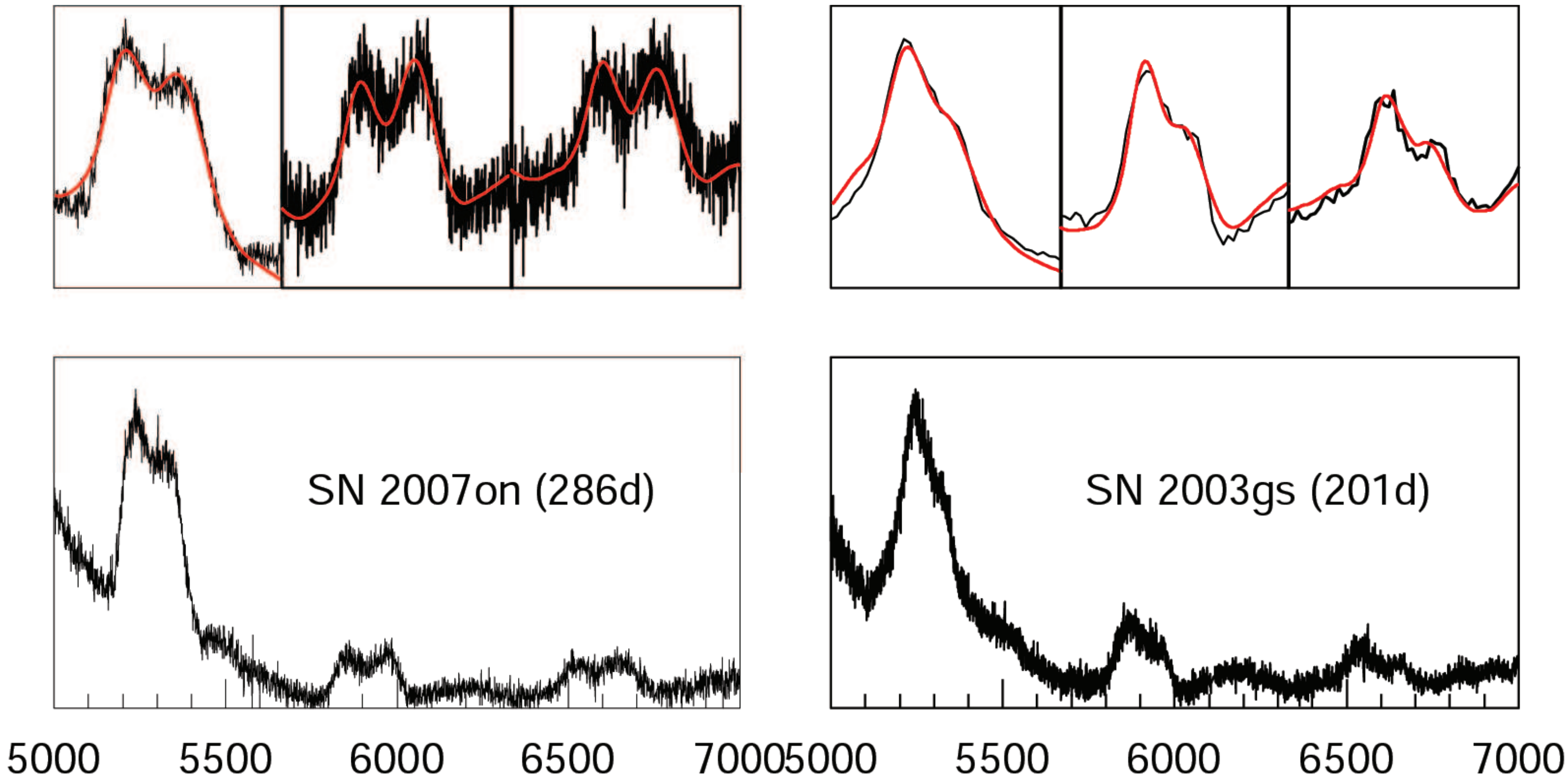

Dong et al. (2014):

- The two peaks are respectively blue-shifted and red-shifted relative to the host galaxies and are separated by ~ 5000 km s^{-1}.
- Bi-modality is naturally expected from direct collision of white dwarfs due to the detonation of both white dwarfs.

Abundances in 20 $M_\odot$ star at late stage

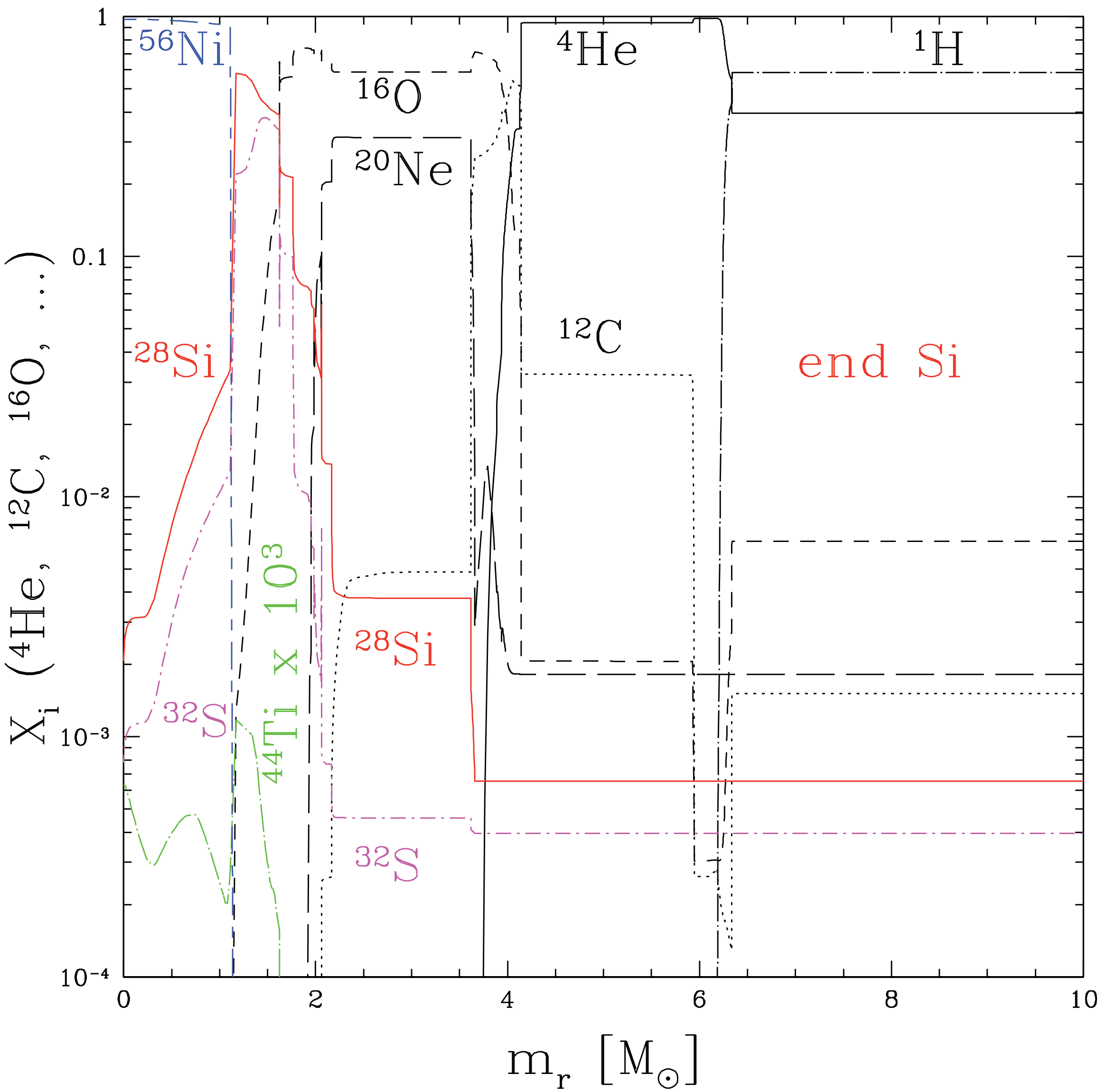

Hirschi et al. (2004)

Radial velocity profiles for the collapse

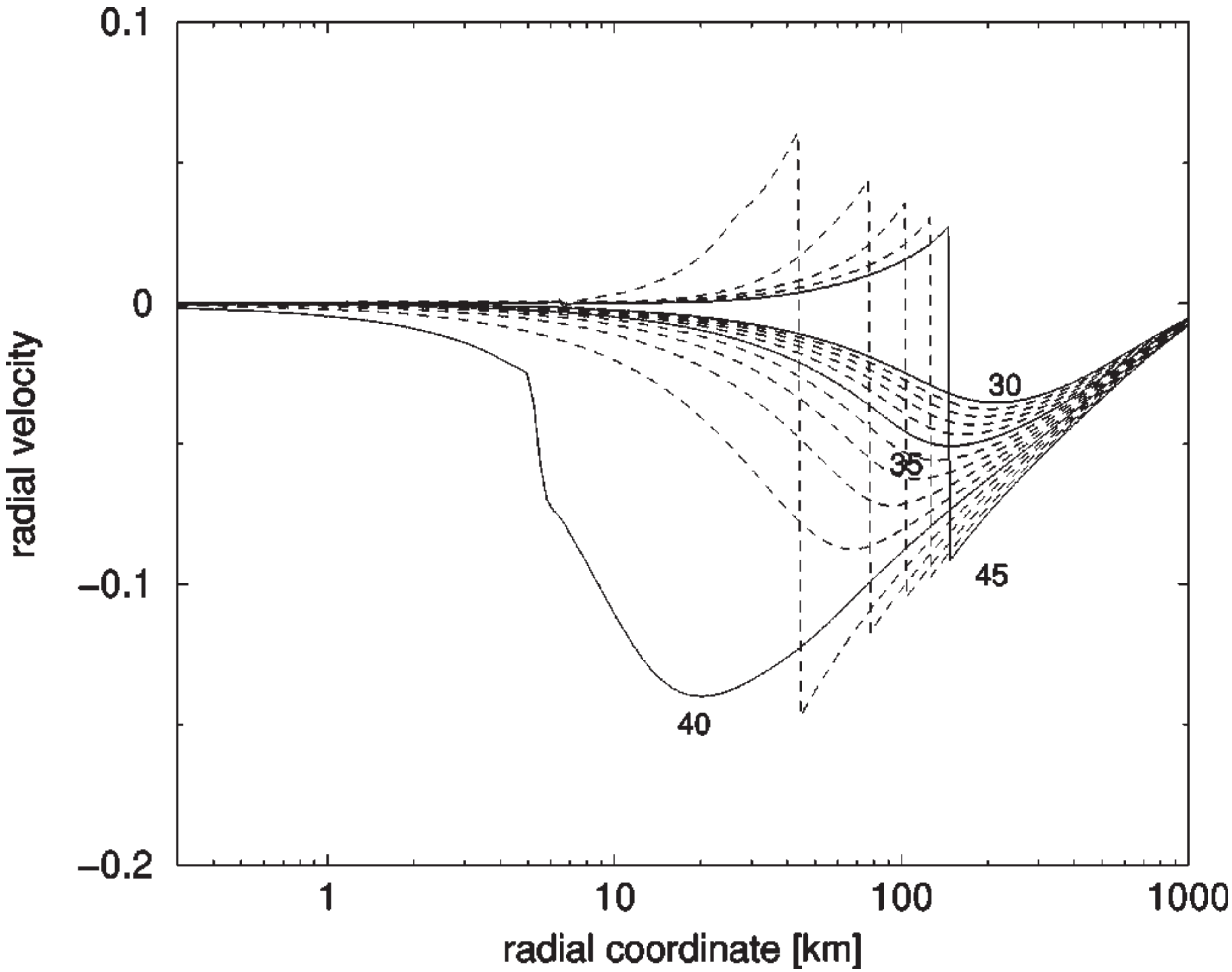

The gravitational collapse occurs when $\Gamma = (\partial \ln P / \partial \ln \rho)_S < 4/3$
Siebel et al. (2003)

The adiabatic index

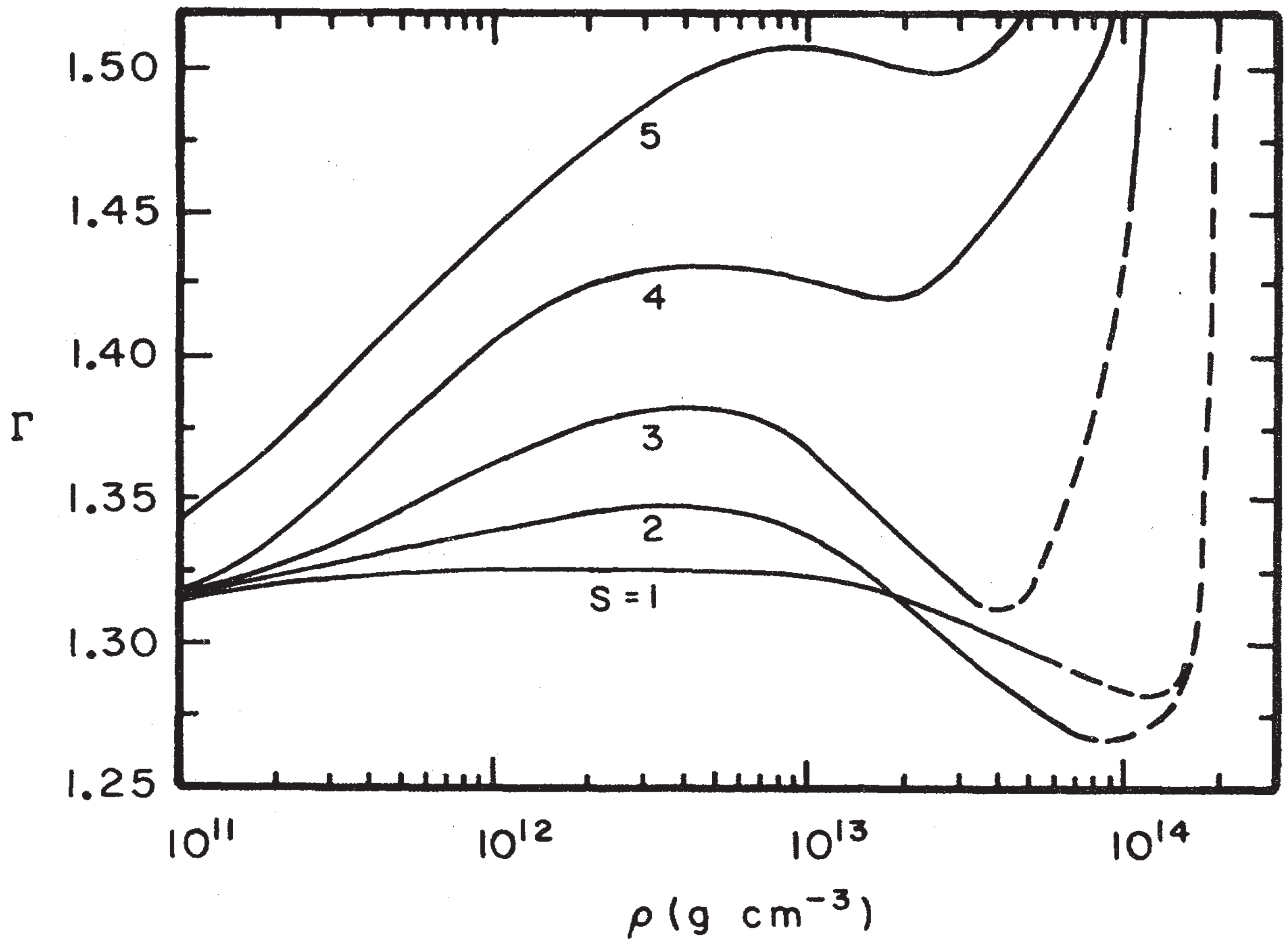

The gravitational collapse runs with S ∼ 1.
Bethe (1990)

Stellar collapse and prompt explosion

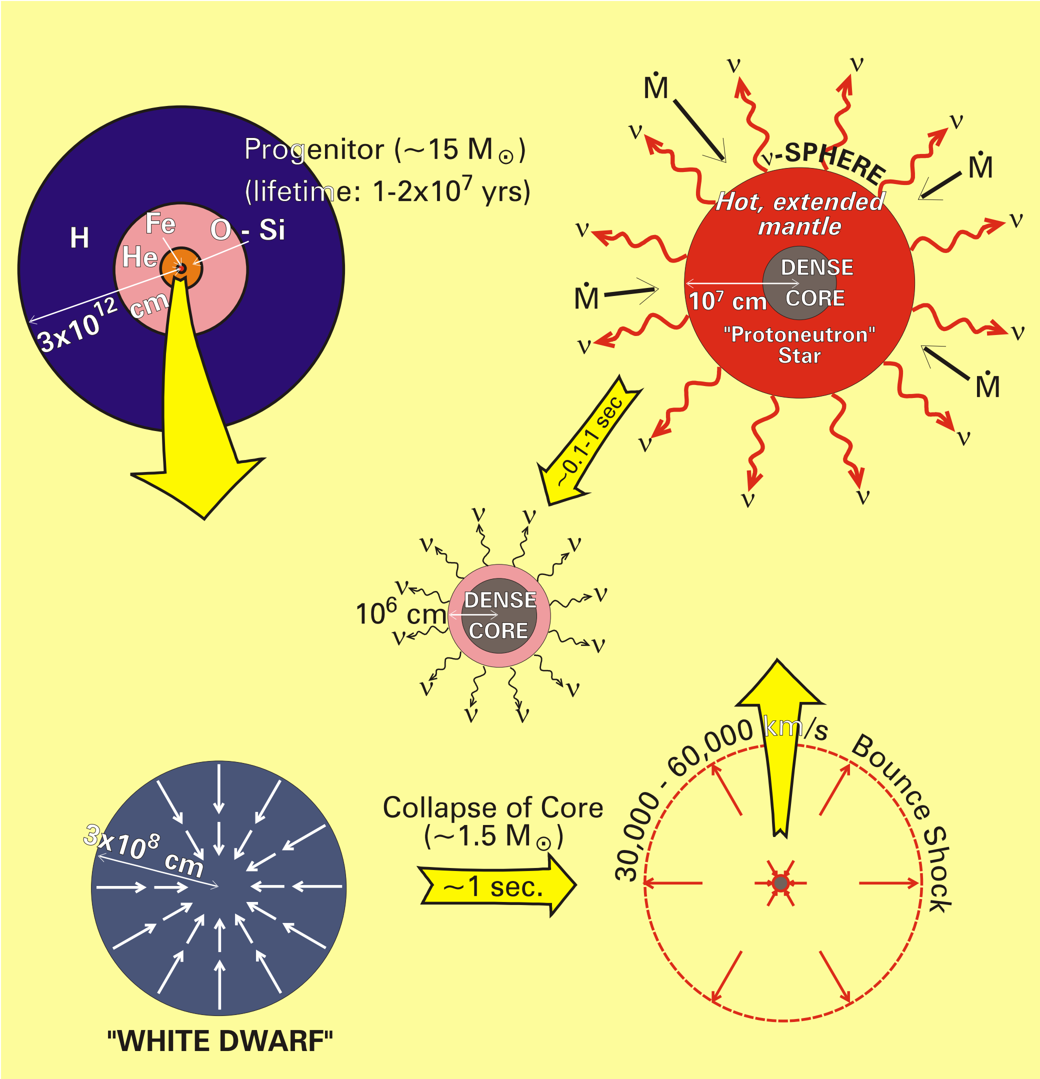

$$E^i_{shock} \approx 6 \times 10^{51} \text{ erg}, \; E_{loss} \approx 1.7 \times 10^{51} (M_{\rm Fe}/0.1 M_\odot) \text{ erg}$$

Burrows (2012)

Stalled supernova shock after core bounce

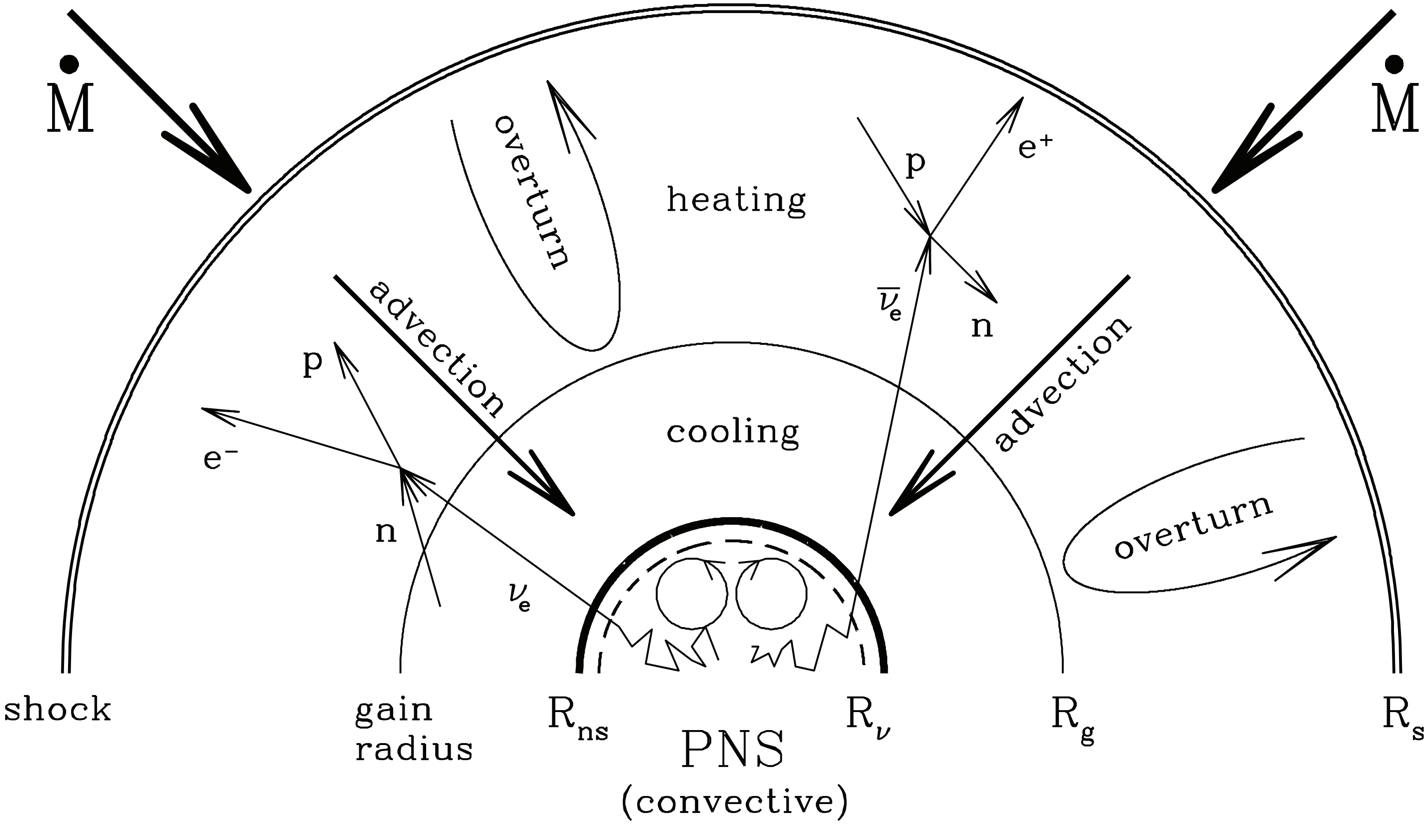

Janka (2001)

Delayed neutrino-heating mechanism (Colgate & White 1966).
Multidimensional problem.
Convection in PNS (Bruenn et al. 1979) and behind the shock (Bethe 1990).

The Neutrino-Driven Mechanism in its Modern Flavour

- Stalled accretion shock pushed out to ~150km as matter piles up on the PNS, then recedes again
- *Heating* or *gain* region develops some tens of ms after bounce
- Convective overturn & shock oscillations “SASI” enhance the efficiency of ν-heating, which finally revives the shock

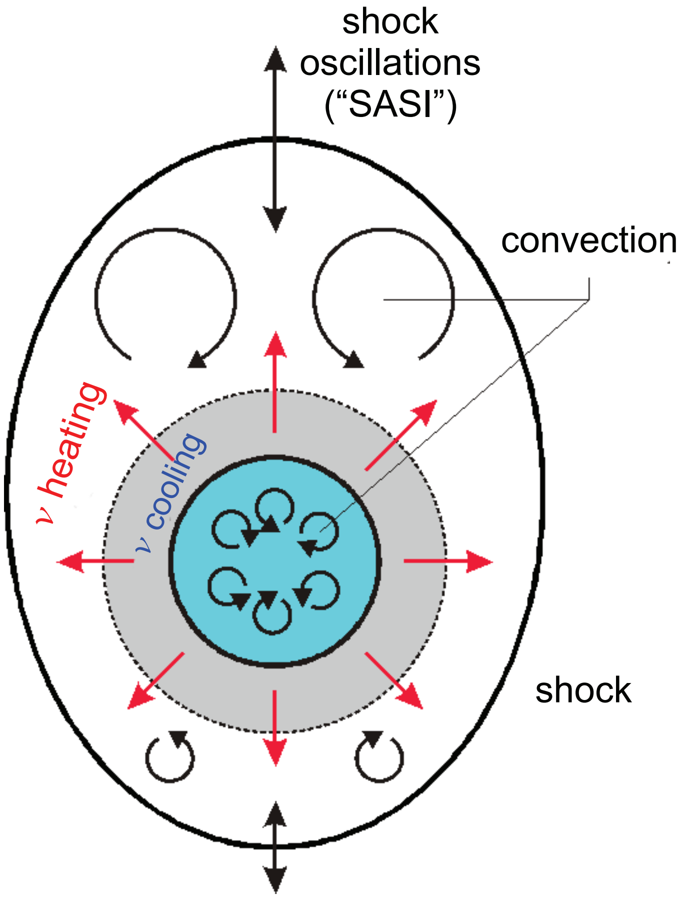

Mueller (2012)

SASI is the so-called Standing Accretion Shock Instability (Blondin et al. 2003).

Multidimensional supernova simulations

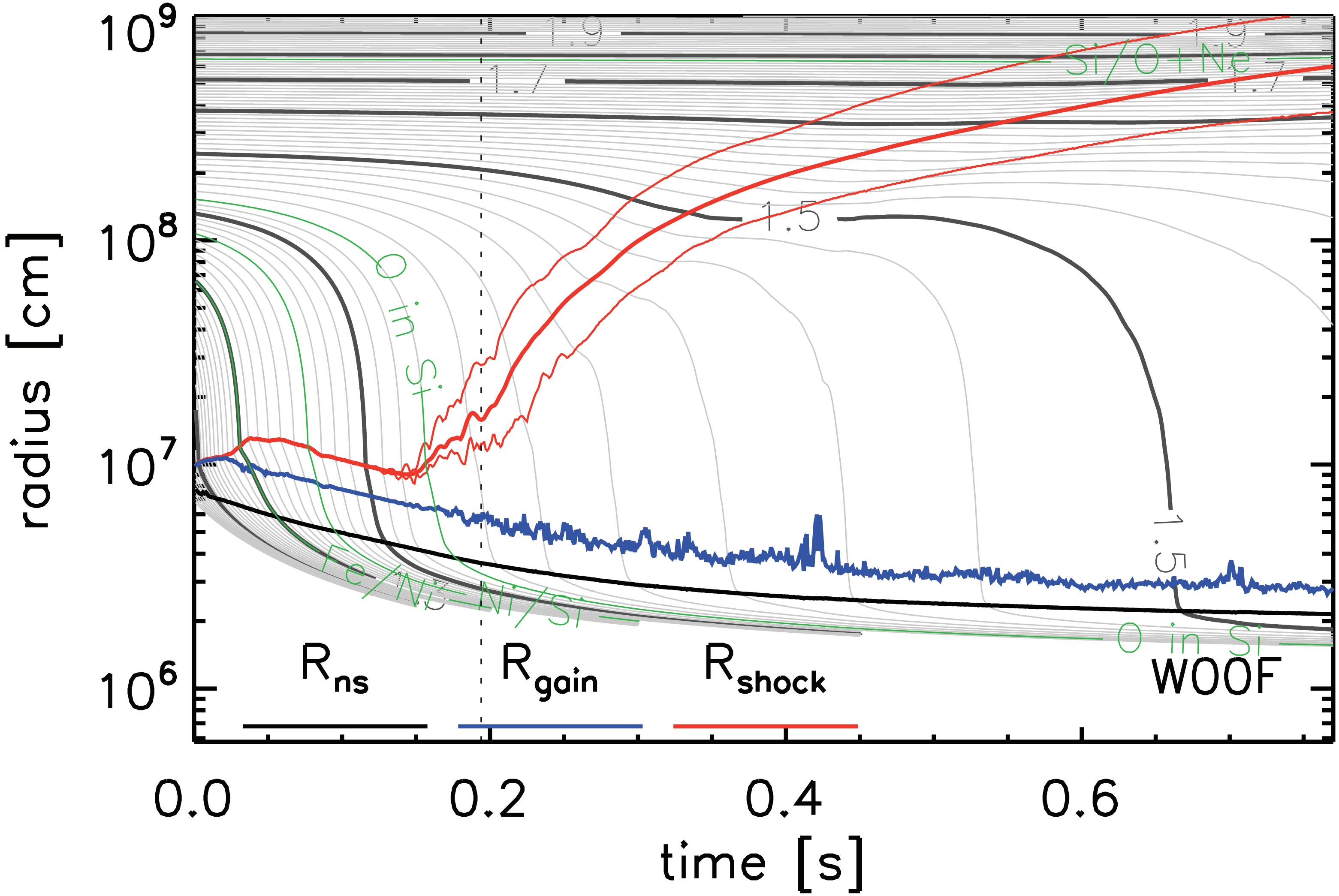

Scheck et al. (2008)

Two-dimensional core collapse supernovae

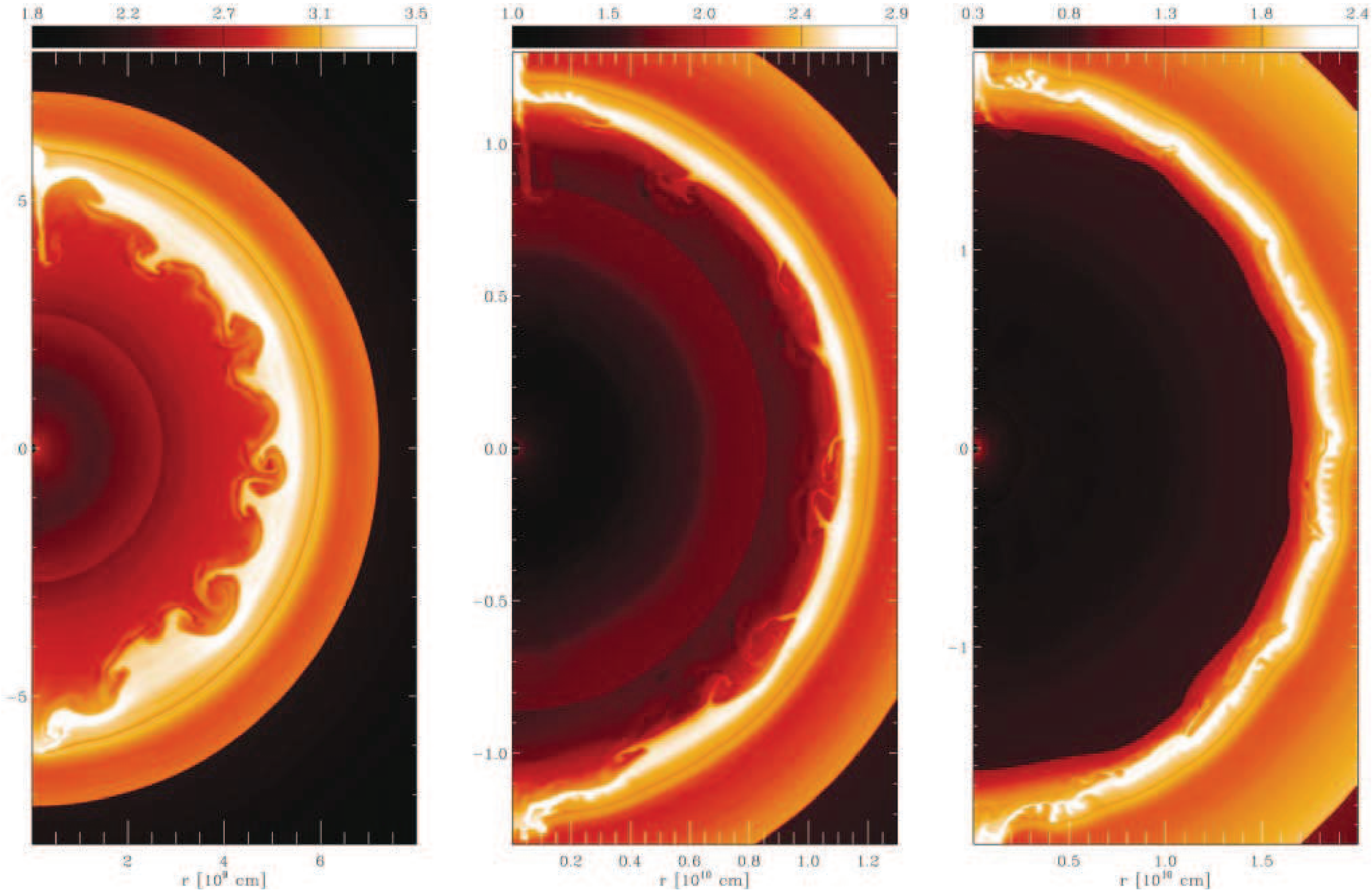

t = 4, 10, and 20 s.
Kifonidis et al. (2003)

Two-dimensional core collapse supernovae

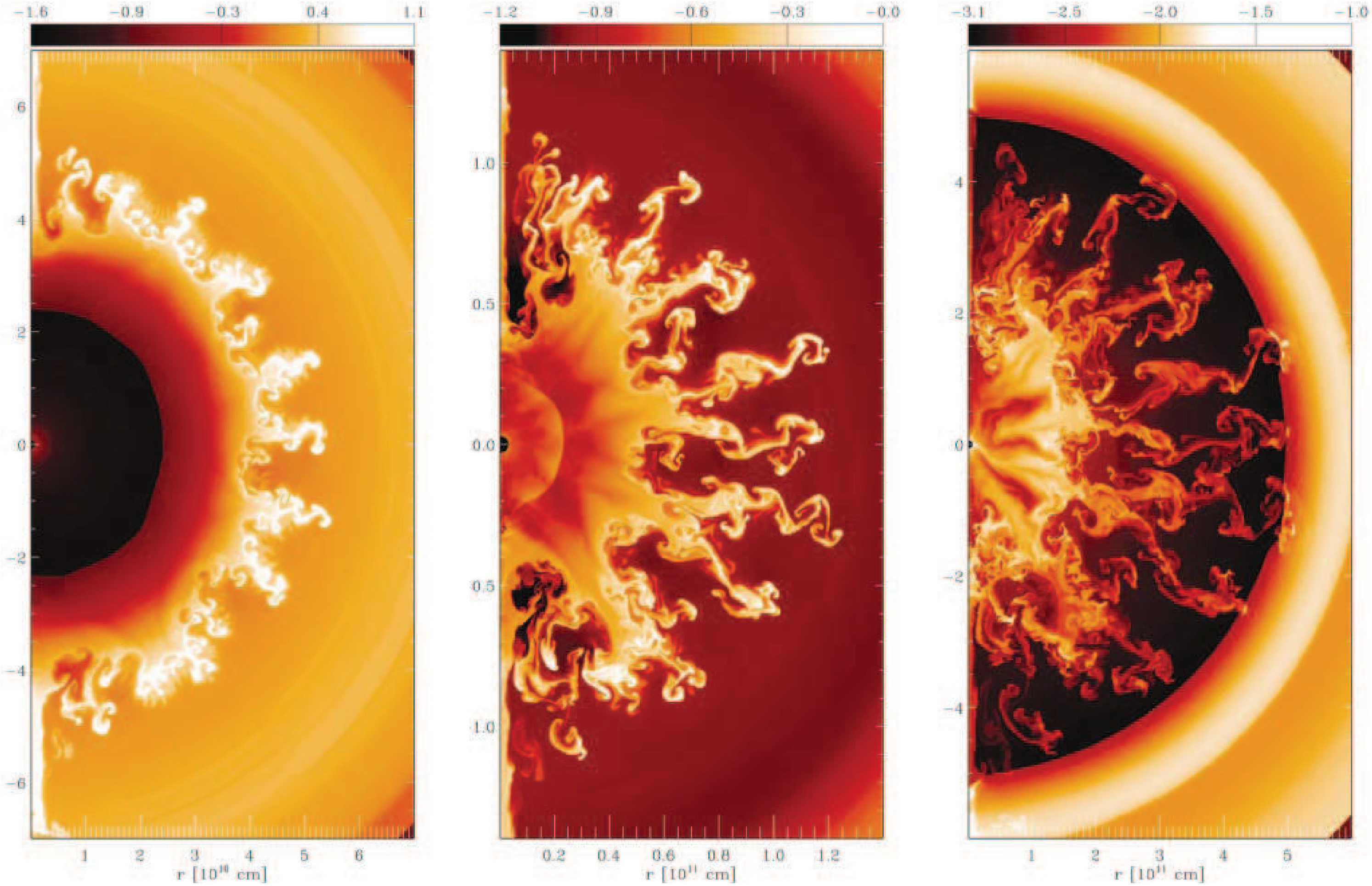

t = 100, 300, and 1500 s.
Kifonidis et al. (2003)

Two-dimensional core collapse supernovae

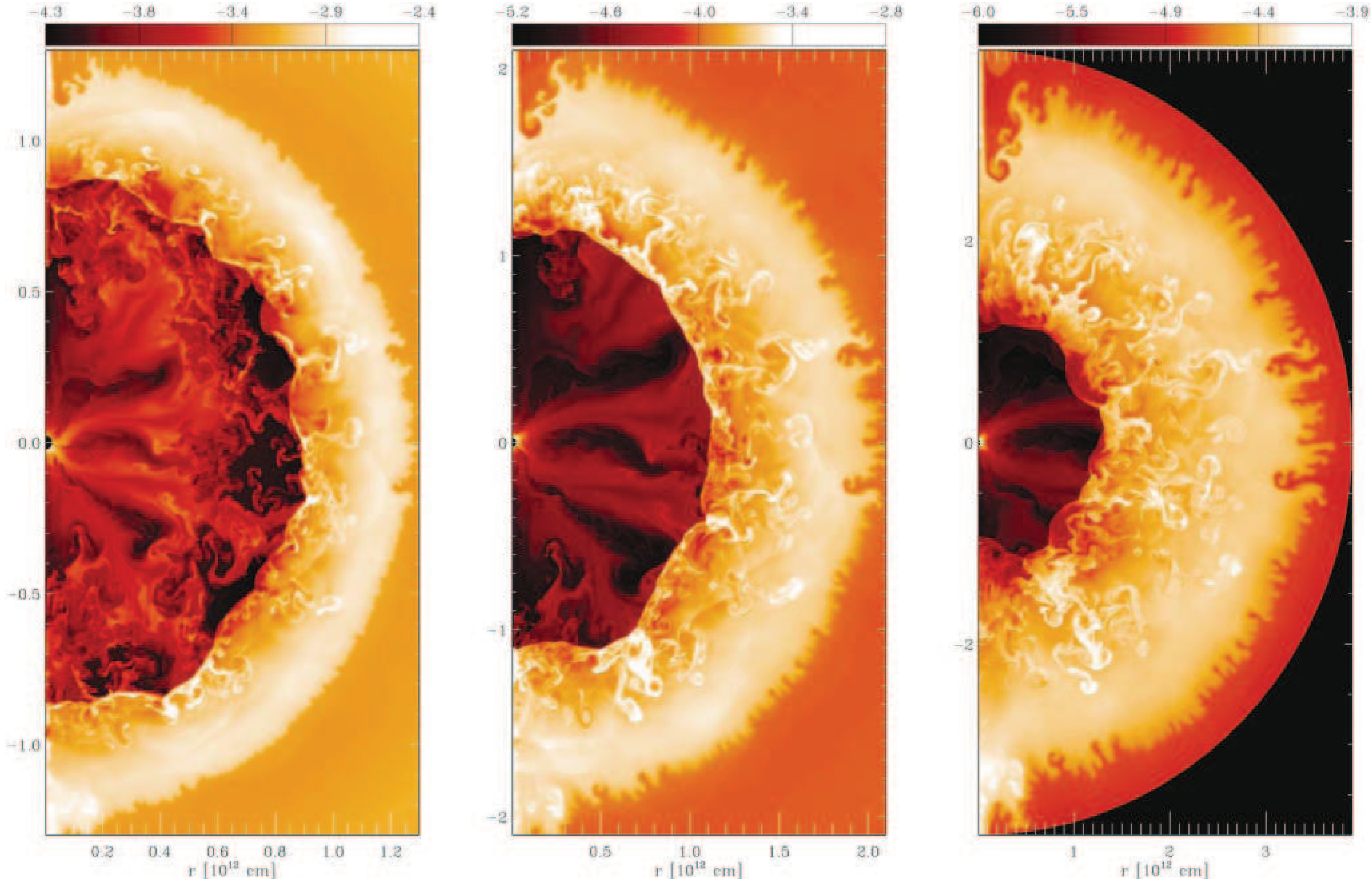

t = 5000, 10 000, and 20 000 s.
Kifonidis et al. (2003)

3D models of supernova explosions

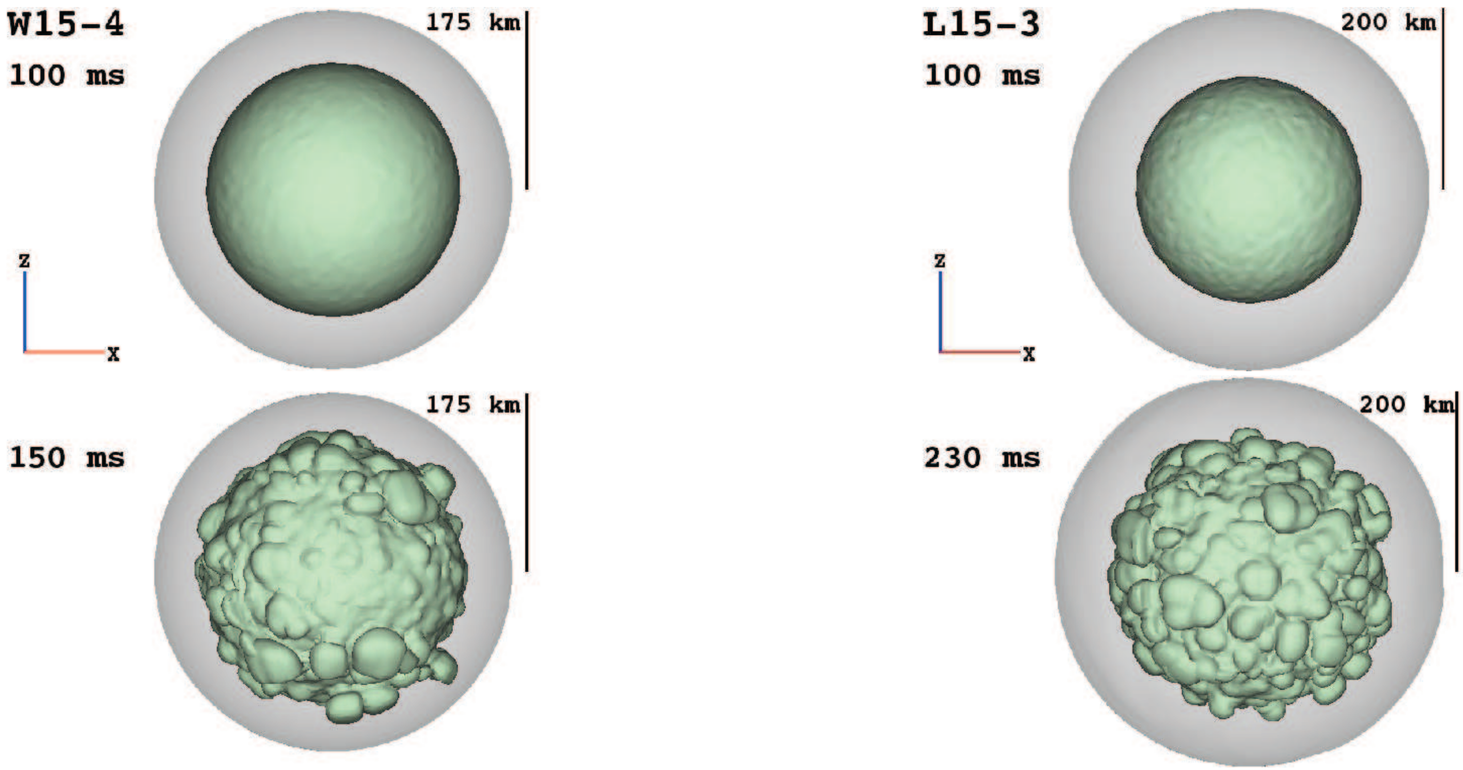

Each snapshot shows two surfaces of constant entropy.
Shock wave – gray and non-radial structure – greenish.
Mueller et al. (2012)

3D models of supernova explosions

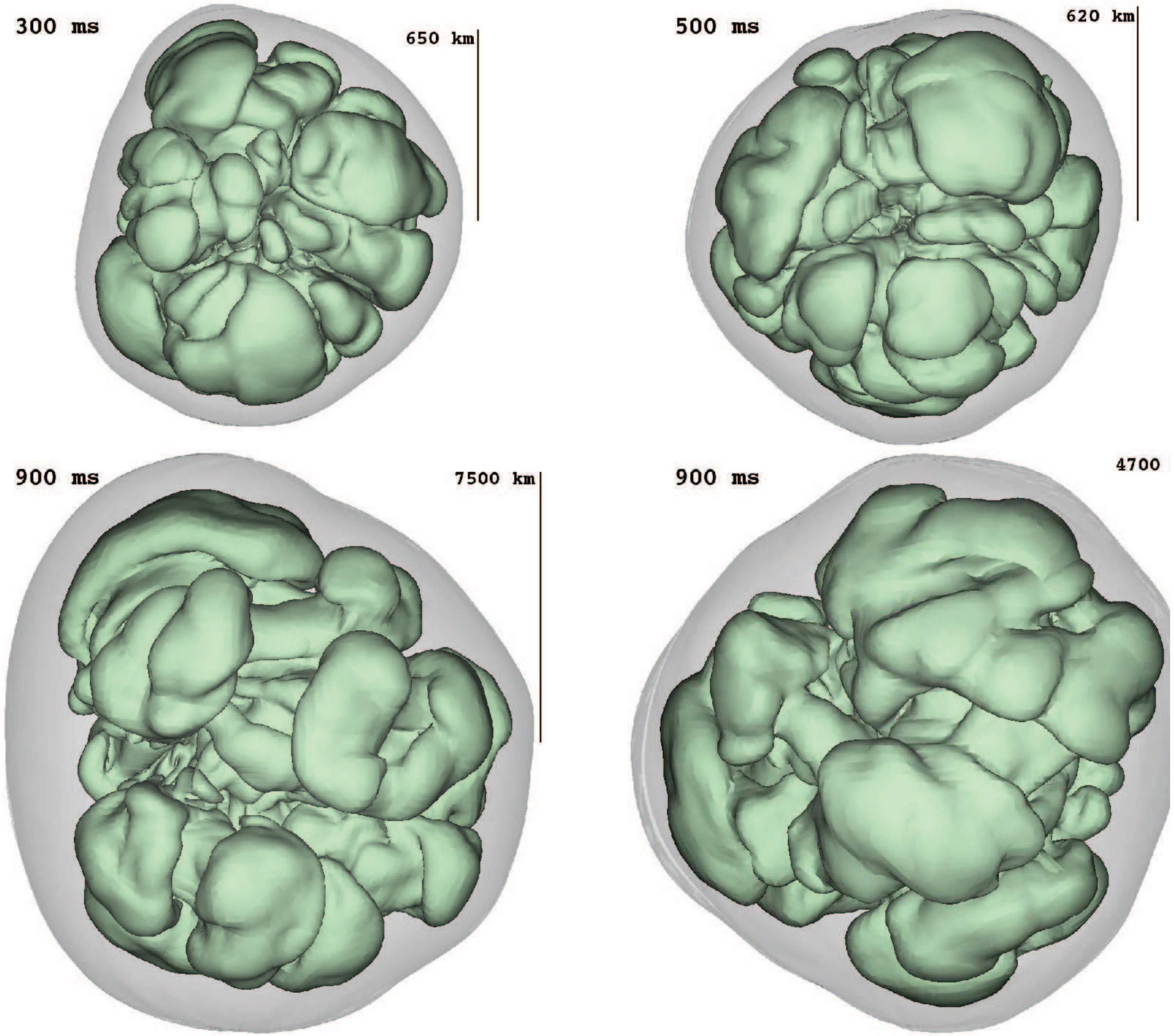

Each snapshot shows two surfaces of constant entropy.
Shock wave – gray and non-radial structure – greenish.
Mueller et al. (2012)

Neutrino luminosities as a function of time

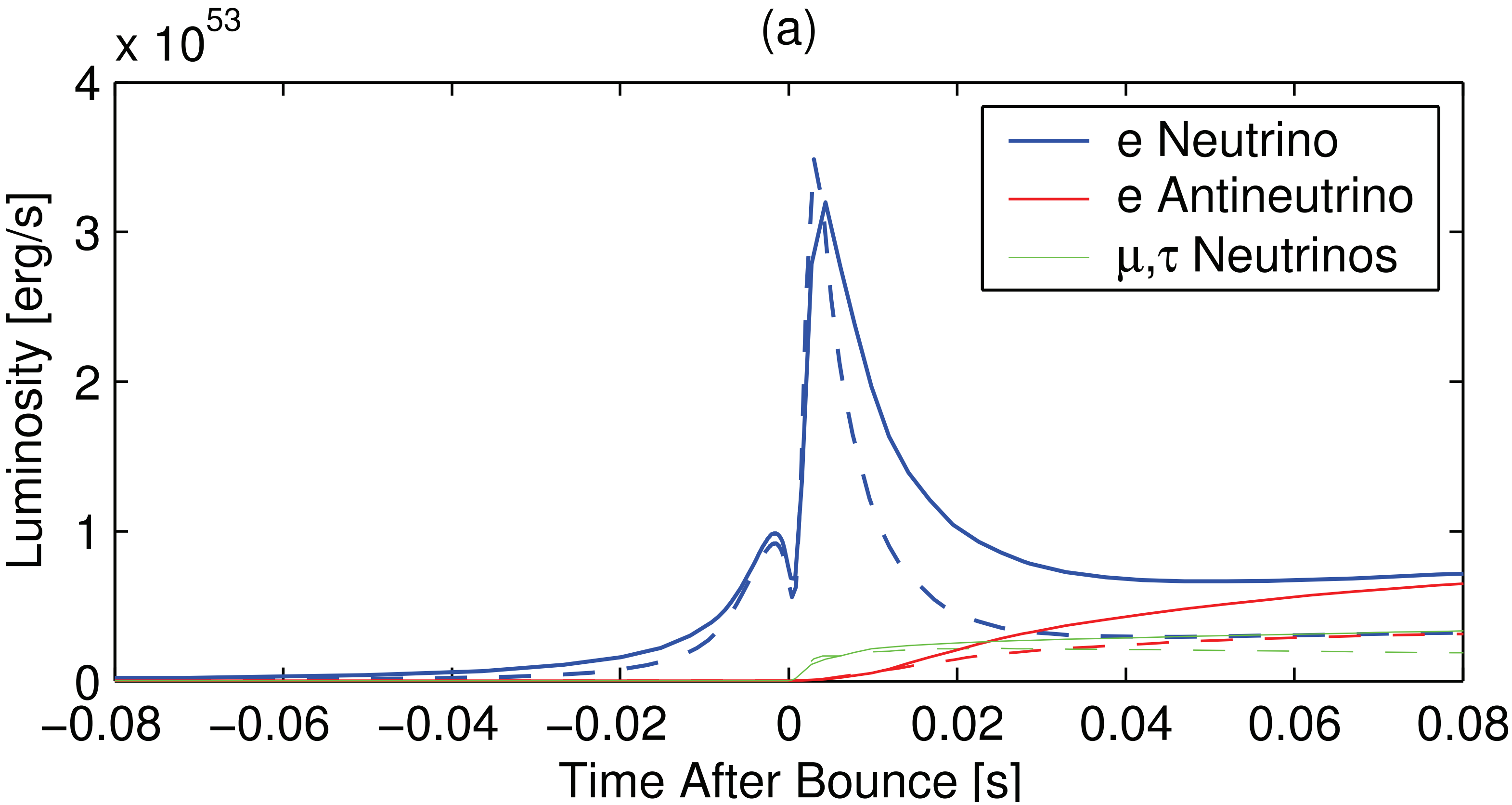

Dashed lines – 13 $M_\odot$ model, solid lines – 40 $M_\odot$ model.
Kotake et al. (2006)

Discovery

Discovered on 24 Feb 1987

Brightest SN since 1604 (Kepler's SN)

Located in the LMC (~ 50 kpc)

Magnitude at maximum +3

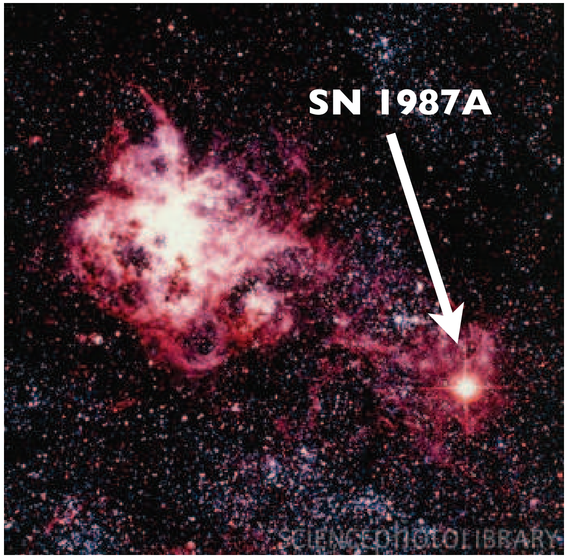

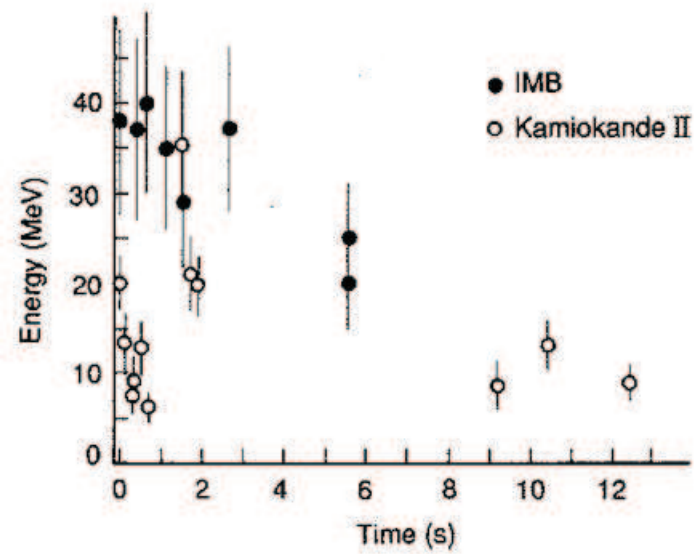

Neutrinos arrived at 23.316 UT (before the optical discovery)

19 neutrinos in 13 s

Confirmed core-collapse scenario

Larsson (2012)

The progenitor

First time a supernova progenitor was identified in pre-explosion images.

The progenitor turned out to be a **Blue Supergiant,** Sk -69 202

Red supergiant had been expected!

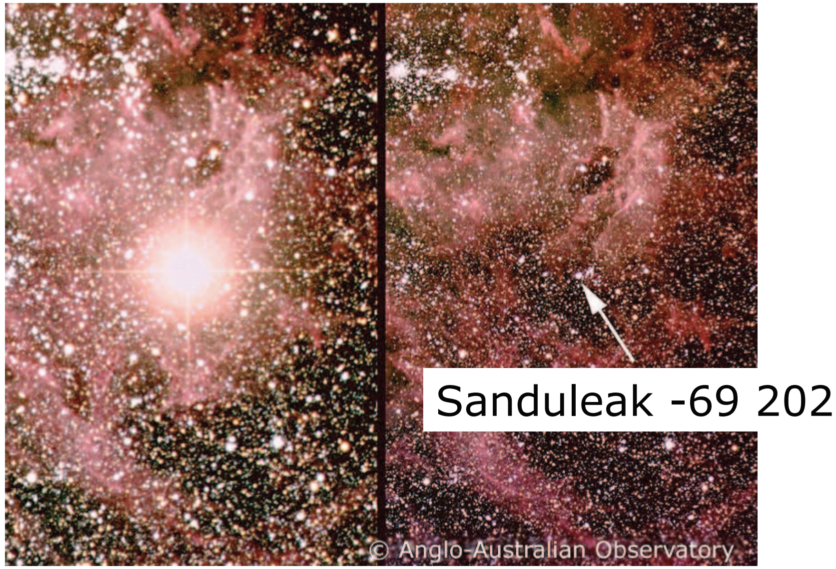

Previous observations of the star had not revealed anything peculiar

Luminosity ~ $10^5\ L_\odot$

Temperature ~ 16 000 K

Radius ~ 40 $R_\odot$

Main sequence mass ~ 16 - 22 $M_\odot$

Larsson (2012)

Bolometric light curve of SN 1987A

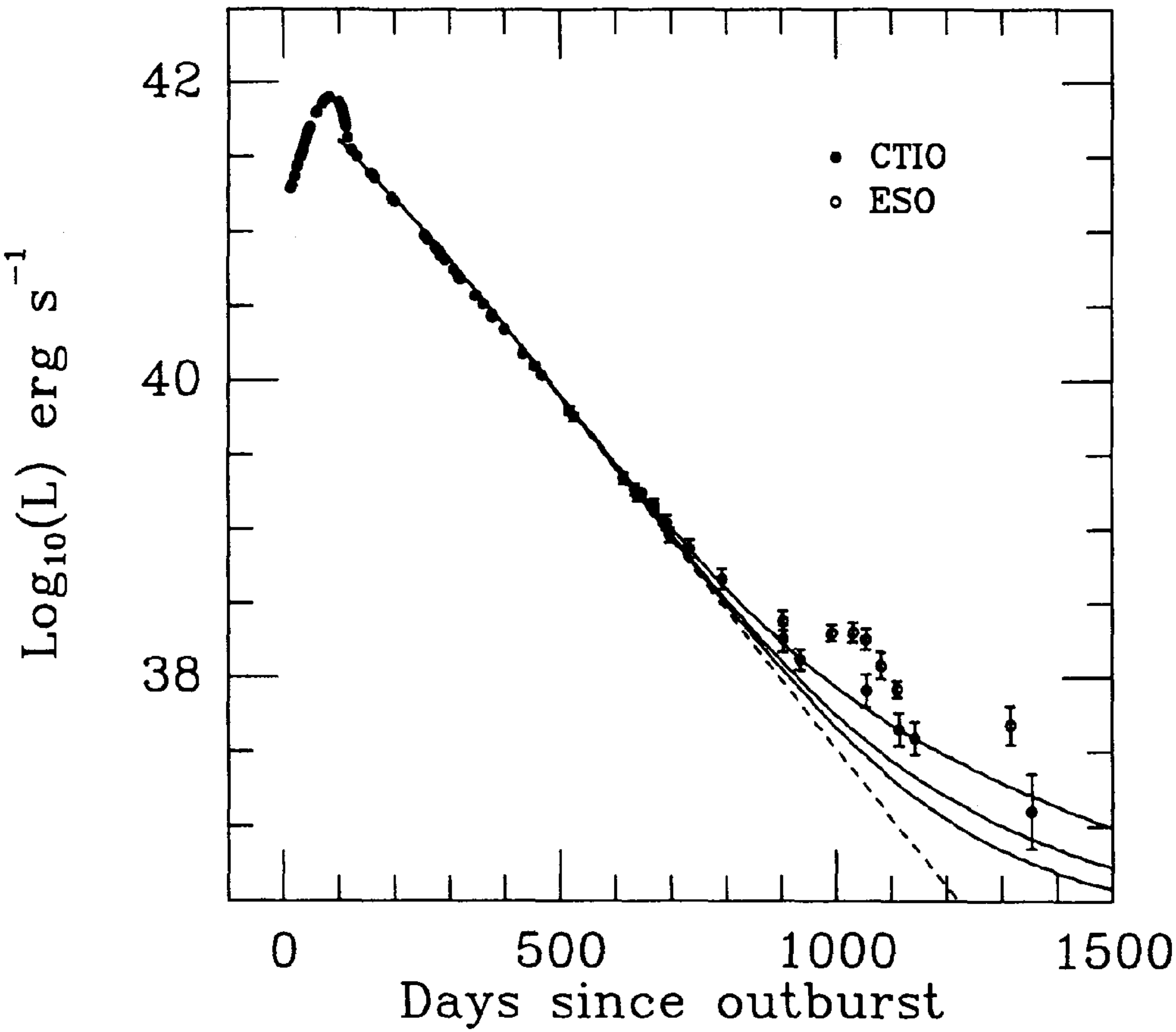

Suntzeff et al. (1991)

Main radioactive decays in SN 1987A

Decay				Time scale	Epoch when dominating
^{56}Ni	$\rightarrow$	^{56}Co + γ		8.8 d	0–18 d
		^{56}Co	$\rightarrow$ ^{56}Fe + γ	111.3 d	18–1100 d
			$\rightarrow$ ^{56}Fe + e^+		
^{57}Ni	$\rightarrow$	^{57}Co + γ		2.17 d	
		^{57}Co	$\rightarrow$ ^{57}Fe + γ	390 d	1100–1800 d
^{44}Ti	$\rightarrow$	^{44}Sc + γ		87 yrs	1800 d $\rightarrow$
		^{44}Sc	$\rightarrow$ ^{44}Ca + γ	5.4 h	
			$\rightarrow$ ^{44}Ca + e^+		

γ-ray spectrum from SN 1987A

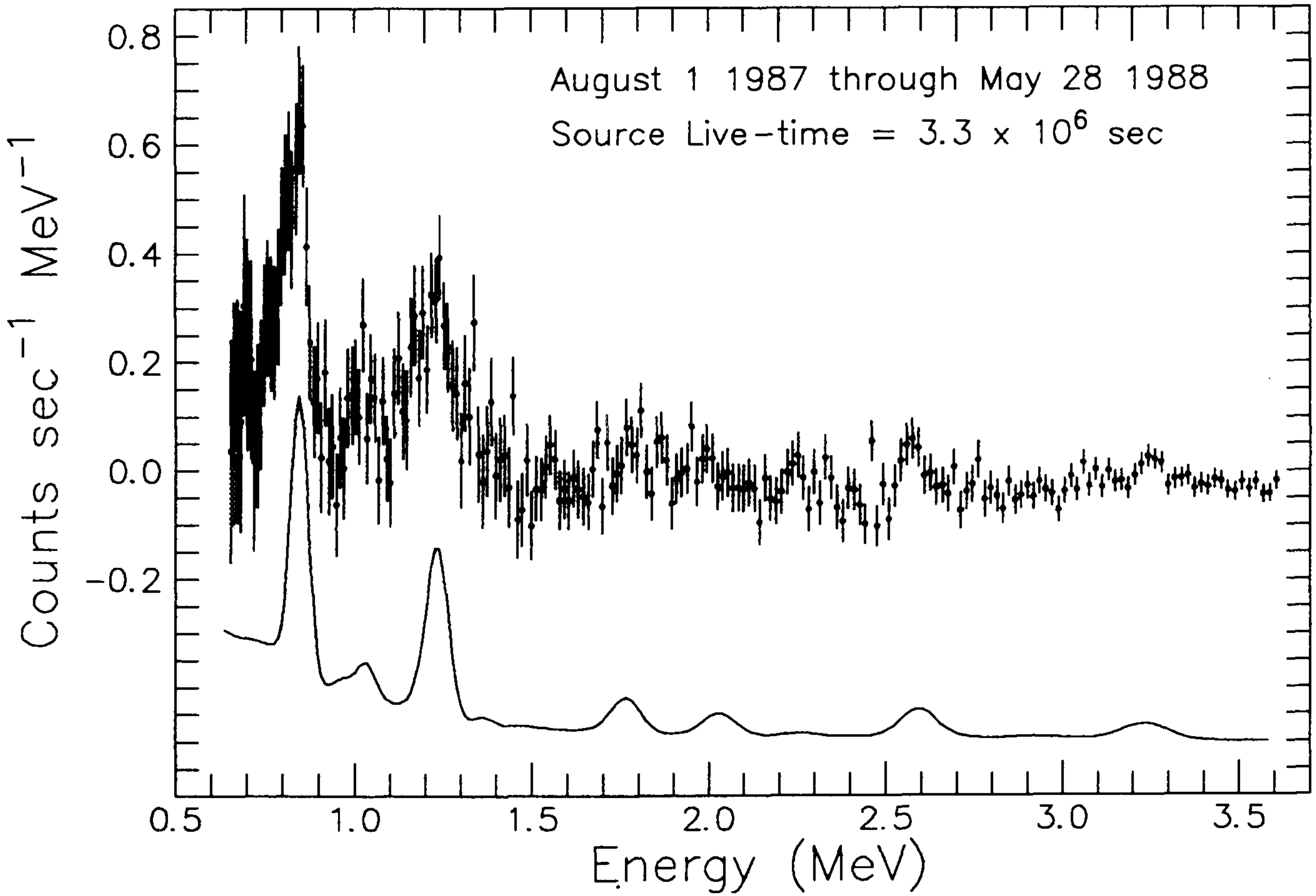

Monte Carlo simulations of the 847, 1238, 2599, and 3250 keV lines.
Leising & Share (1990)

Уравнения радиационной гидродинамики в одногрупповом приближении

Систему уравнений радиационной гидродинамики составляют: уравнение непрерывности

$$\frac{\partial r}{\partial t} = u\ ,\ \frac{\partial r}{\partial m} = \frac{1}{4\pi r^2 \rho}\ ,$$

уравнение движения

$$\frac{\partial u}{\partial t} = -4\pi r^2 \frac{\partial (P_g + Q)}{\partial m} - \frac{Gm}{r^2} + \frac{1}{c}\chi_F^0 F^0\ ,$$

уравнение энергии для газа

$$\frac{\partial E_g}{\partial t} = -(P_g + Q)\frac{\partial}{\partial t}\left(\frac{1}{\rho}\right) + c\kappa_E^0 E^0 - 4\pi \frac{\eta_t^0}{\rho} + \varepsilon\ ,$$

уравнение для полной плотности энергии излучения

$$\frac{\partial E^0}{\partial t} = -4\pi\rho \frac{\partial (r^2 F^0)}{\partial m} - 4\pi\rho(1+f^0)E^0 \frac{\partial (r^2 u)}{\partial m} + \frac{u}{r}(3f^0 - 1)E^0 + 4\pi\eta_t^0 - c\rho\kappa_E^0 E^0\ ,$$

и уравнение для полного потока энергии излучения

$$\frac{\partial F^0}{\partial t} = \left(2\frac{u}{r} - c\rho\chi_F^0 - 8\pi\rho\frac{\partial (r^2 u)}{\partial m}\right)F^0 - c^2\left(4\pi r^2 \rho \frac{\partial (f^0 E^0)}{\partial m} + \frac{1}{r}(3f^0 - 1)E^0\right)\ .$$

Ионизационное равновесие и уравнение состояния

Уравнение ионизационного баланса для атома Z^0 и иона Z^+, в котором скорости фотоионизации, ионизации электронами и нетепловой ионизации уравновешиваются скоростями излучательной и трехчастичной рекомбинаций, имеет вид

$$R_{\mathrm{Z}^0} N_{\mathrm{Z}^0} + q_{\mathrm{Z}^0} N_e N_{\mathrm{Z}^0} + \Gamma_{\mathrm{Z}^0} N_{\mathrm{Z}^0} = \alpha_{\mathrm{Z}^+} N_e N_{\mathrm{Z}^+} + \chi_{\mathrm{Z}^+} N_e^2 N_{\mathrm{Z}^+} \ .$$

Давление P_g и внутренняя энергия идеального газа E_g, составляющие уравнение состояния, для смеси химических элементов равны

$$P_g = \frac{kT_g}{m_u A}(1 + Ax_e)\rho \ ,$$

$$\begin{aligned} E_g \ = \ & \frac{3}{2}\frac{kT_g}{m_u A}(1 + Ax_e) + \frac{X_{\mathrm{H}}}{m_u A_{\mathrm{H}}}\left(I_{\mathrm{H}} x_{\mathrm{H}^+} - I_{\mathrm{H}^-} x_{\mathrm{H}^-}\right) \\ & + \sum_{\mathrm{Z}=\mathrm{He}}^{\mathrm{Fe}} \frac{X_{\mathrm{Z}}}{m_u A_{\mathrm{Z}}}\left(I_{\mathrm{Z}^0} x_{\mathrm{Z}^+} + \left(I_{\mathrm{Z}^0} + I_{\mathrm{Z}^+}\right) x_{\mathrm{Z}^{++}}\right) \ . \end{aligned}$$

Средние непрозрачности и коэффициент излучения

- Относительные концентрации атомов и ионов, вычисленные при отсутствии ЛТР, но без учета возбужденных состояний, определяют соответствующие средние непрозрачности χ_F^0 и κ_E^0 и коэффициент теплового излучения η_t^0. В качестве средней непрозрачности, взвешенной по потоку энергии излучения, χ_F^0 используется росселандово среднее. Средняя непрозрачность, взвешенная по плотности энергии излучения, κ_E^0 вычисляется как планковское среднее с температурой излучения T_r.
- Более 500000 спектральных линий были выбраны из обширной базы атомных данных, которую составили Kurucz & Bell (1995). Все они были использованы при усреднении вклада спектральных линий в непрозрачность вещества в оболочке сверхновой, расширяющейся с градиентом скорости.

Optimal hydrodynamic model for SN 1987A

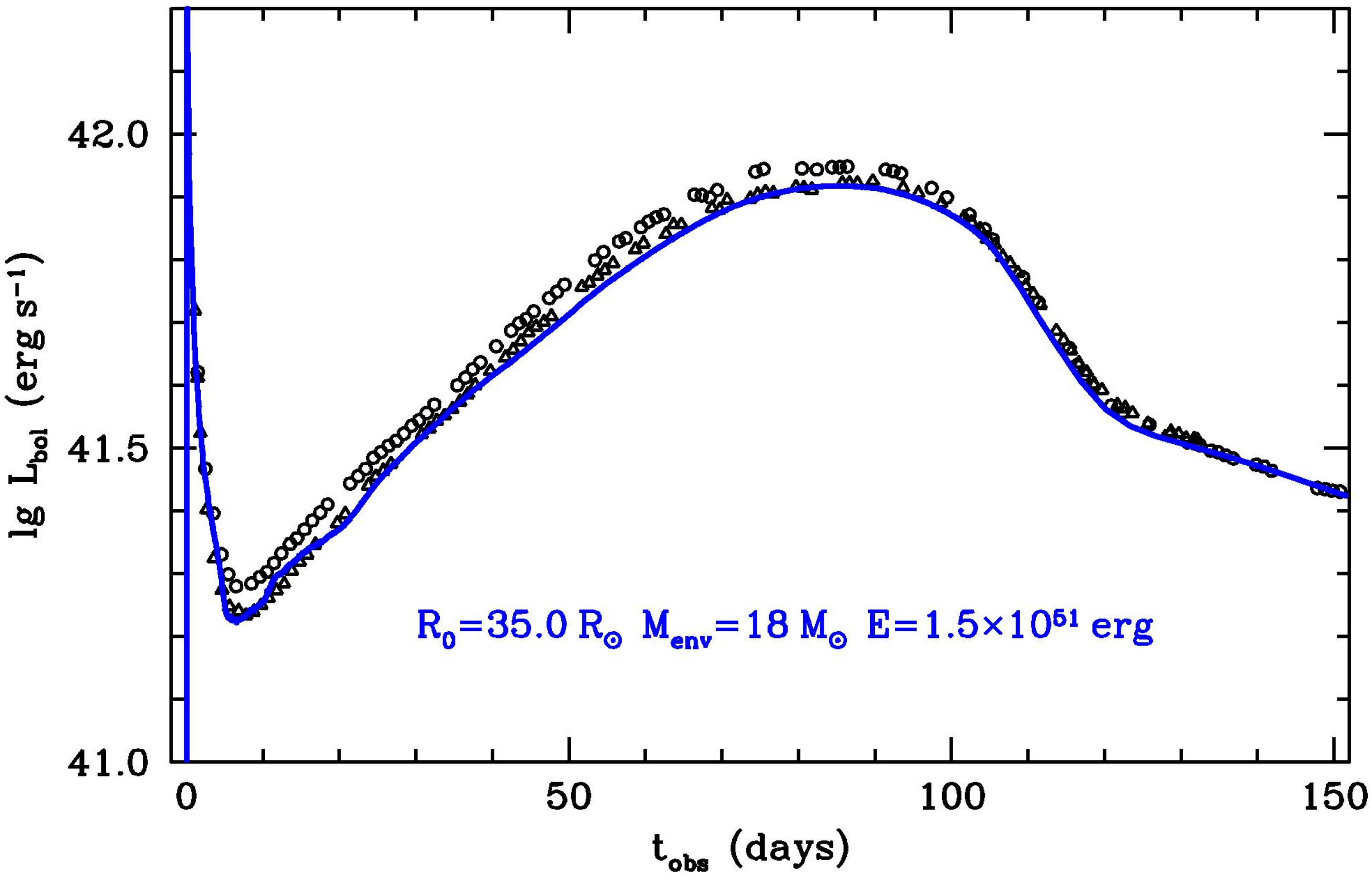

Detection of the SN 1987A rings

ESO New Technology Telescope (1990) and Hubble Space Telescope (1991)

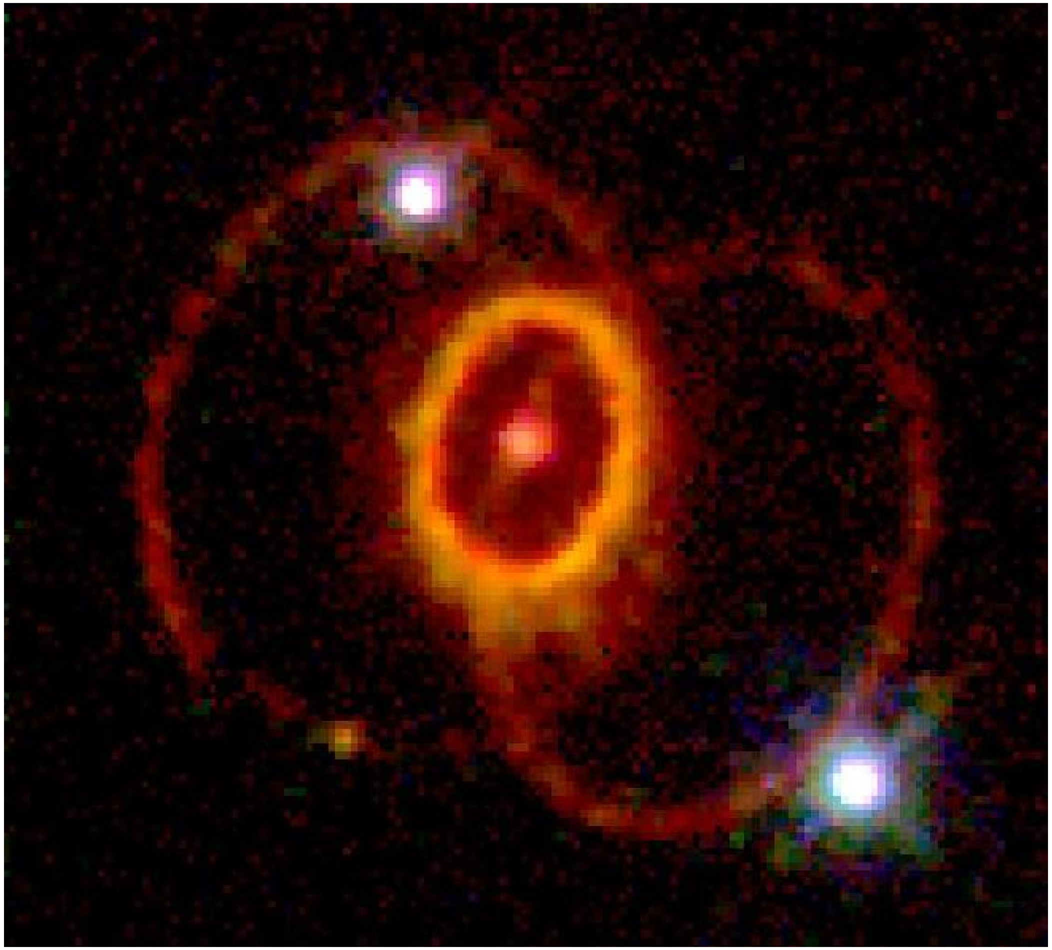

Hubble Space Telescope (1995)

The Mysterious Rings of Supernova 1987A

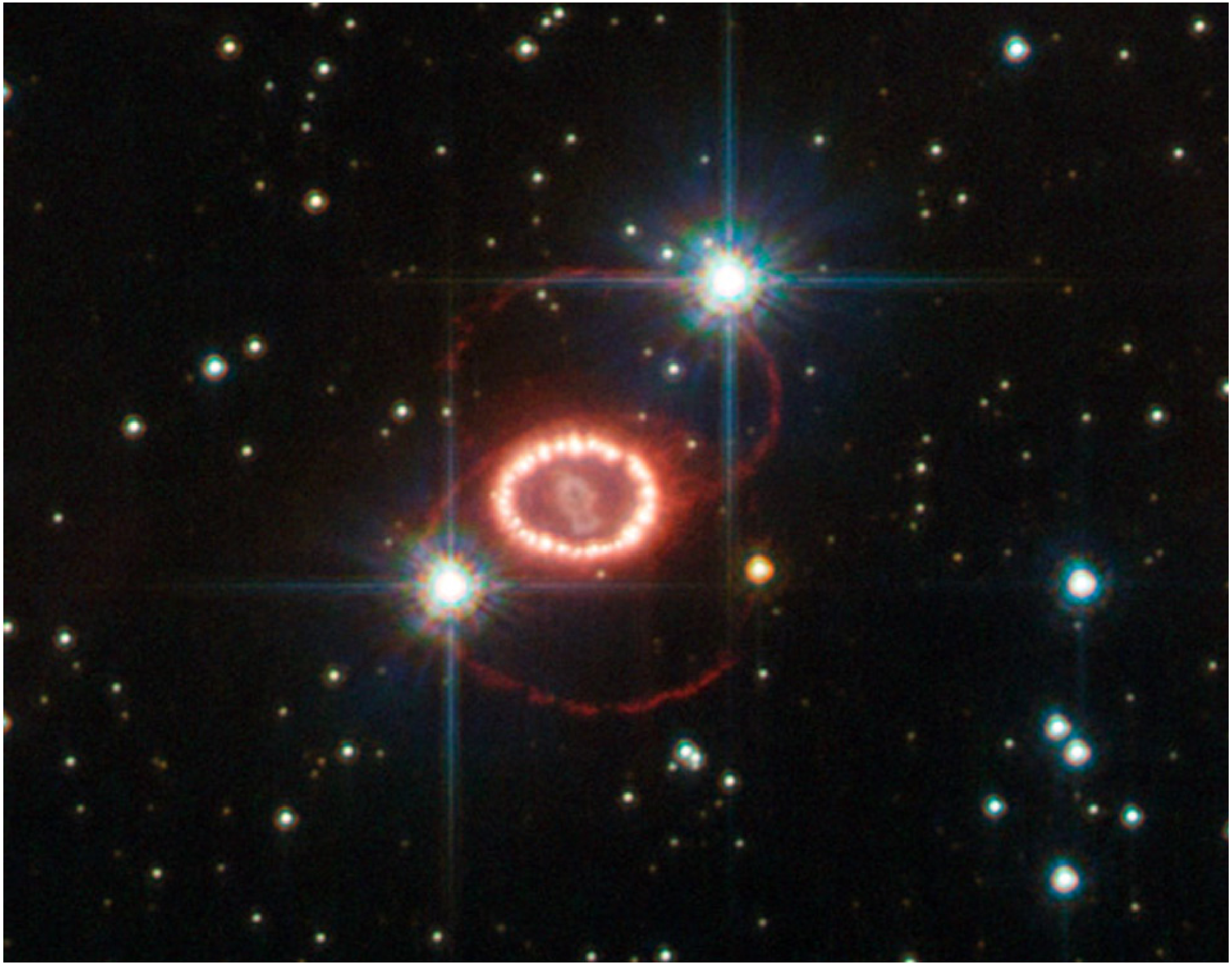

ESA/Hubble, NASA (2012)